haematologica
Journal of the Ferrata Storti Foundation

A small molecule inhibitor of RNA-binding protein IGF2BP3 shows anti-leukemic activity

by Amit K. Jaiswal, Georgia M. Scherer, Michelle L. Thaxton, Jacob P. Sorrentino, Constance Yuen, Milauni M. Mehta, Gunjan Sharma, Tasha L. Lin, Tiffany M. Tran, Amanda Cohen, Alexander J. Ritter, Rishi S. Kotecha, Jeremy R. Sanford, Robert D. Damoiseaux, Neil K. Garg and Dinesh S. Rao

Received: May 14, 2025.
Accepted: November 18, 2025.

Citation: Amit K. Jaiswal, Georgia M. Scherer, Michelle L. Thaxton, Jacob P. Sorrentino, Constance Yuen, Milauni M. Mehta, Gunjan Sharma, Tasha L. Lin, Tiffany M. Tran, Amanda Cohen, Alexander J. Ritter, Rishi S. Kotecha, Jeremy R. Sanford, Robert D. Damoiseaux, Neil K. Garg and Dinesh S. Rao.
A small molecule inhibitor of RNA-binding protein IGF2BP3 shows anti-leukemic activity.
Haematologica. 2025 Nov 27. doi: 10.3324/haematol.2025.288221 [Epub ahead of print]

A small molecule inhibitor of RNA-binding protein IGF2BP3 shows anti-leukemic activity

Amit K. Jaiswal[1], Georgia M. Scherer[2*], Michelle L. Thaxton[1*], Jacob P. Sorrentino[2], Constance Yuen[3], Milauni M. Mehta[2], Gunjan Sharma[1], Tasha L. Lin[1], Tiffany M. Tran[1], Amanda Cohen[1], Alexander J. Ritter[4], Rishi S. Kotecha[5,6,7], Jeremy R. Sanford[4,8], Robert D. Damoiseaux[3,9,10,11,] Neil K. Garg[2] and Dinesh S. Rao[1,11,12]

Contributions: * G.M.S and M.L.T contributed equally as second authors to this manuscript.

Affiliations:

[1] Department of Pathology and Laboratory Medicine, University of California, Los Angeles, CA, USA

[2]Department of Chemistry and Biochemistry, University of California, Los Angeles, CA, USA
[3]California Nanosystems Institute, University of California, Los Angeles, CA, USA
[4] Department of Molecular, Cell and Developmental Biology and Center for Molecular Biology of RNA, University of California, Santa Cruz, CA, USA

[5]Department of Clinical Haematology, Oncology, Blood and Marrow Transplantation, Perth Childrens Hospital, Perth, Australia

[6]Leukemia Translational Research Laboratory, WA Kids Cancer Centre, University of Western Australia, Perth Australia

[7]Curtin Medical School, Curtin University, Perth, Australia
[8]Center for Biomolecular Science & Engineering, University of California, Santa Cruz, CA, USA
[9]Department of Molecular and Medical Pharmacology, University of California, Los Angeles, CA, USA

[10]Department of Bioengineering, Samueli School of Engineering, University of California, Los Angeles, CA, USA

[11]Jonsson Comprehensive Cancer Center, University of California Los Angeles, CA, USA
[12]Broad Stem Cell Research Center, University of California Los Angeles, CA, USA

Running Title: IGF2BP3 small molecule inhibitors in leukemia

Corresponding Author:
Dinesh S. Rao, M.D., Ph.D.,
Professor
Department of Pathology and Laboratory Medicine
David Geffen School of Medicine at UCLA
Email drao@mednet.ucla.edu

Data Sharing Statement: High throughput sequencing data has been deposited in the NCBI Short Read Archive (BioProject PRJNA1333638 and PRJNA1336320), and will be released upon publication. Methodologies are documented in the supplementary materials and further information can be provided by the corresponding author. Biological or chemical materials that were created in the process of this work can be requested from the corresponding author and will be released following compliance with relevant intellectual property and material transfer policies.

Trial Registration: NA

Acknowledgments:

We thank Dr. Stuart Conway and Keefe Oei for helpful conversations, advice and protocols for biophysical assays. We thank Jaspal Bassi and Dr. John Colicelli, for helpful discussions regarding the research.

Funding:

This work was supported by CIRM DISC-2-13456 from the California Institute of Regenerative Medicine (DSR), R01CA264986 from the National Institutes of Health (DSR, JRS), R03CA251854 (DSR), the Jonsson Comprehensive Cancer Center (JCCC) (DSR), the Gary & Barbara Luboff Mitzvah Fund (DSR) and the UCLA Innovation Fund Award (DSR). Flow cytometry was performed in the UCLA JCCC and Center for AIDS Research Flow Cytometry Core Facility that is supported by National Institutes of Health awards AI28697, and award number P30CA016042, the JCCC, the UCLA AIDS Institute, and the David Geffen School of Medicine at UCLA. We are especially indebted to the Molecular Screening Shared Resource team for setup and execution of small molecule related screening assays. The MSSR is also supported by the Jonsson Comprehensive Cancer Center (NIH award number P30CA016042, Cancer Center Support Grant). These studies were also supported by the National Science Foundation (DGE-2034835 for GMS and DGE-1650604 for MMM), shared instrumentation grants from the NSF (CHE-1048804), the National Center for Research Resources (S10RR025631), and the NIH Office of Research Infrastructure Programs (S10OD028644).

Conflict of Interest/Disclosures: The corresponding author, Dinesh Rao, serves on advisory boards and has consulted for AbbVie, Inc., a pharmaceutical company that markets drugs for acute leukemia. AKJ, MLT, GMS, JPS, RDD, NKG and DSR are inventors on a patent application that includes the compound I3IN-002.

Author Contributions

A.K.J.: Designed research, Performed experiments, Acquired data, Analyzed data, Generated Figures, Wrote manuscript, Experimental Lead
G.M.S.: Performed experiments, Acquired data, Analyzed data, Assisted in generating figures
M.L.T.: Performed experiments, Acquired data, Analyzed data
J.P.S.: Performed experiments, Acquired data, Analyzed data
C.Y.: Performed experiments
M.M.M.: Performed experiments, Acquired data, Analyzed data
G.S.: Performed experiments
T.M.T.: Performed experiments
T.L.L.: Performed experiments, Acquired data
A.C.: Performed experiments, Acquired data
A.J.R.: Analyzed data
J.R.S.: Analyzed data
R.S.K.: Provided MLL AF4 B-ALL cell line
R.D.D.: Designed research, Analyzed data
N.K.G.: Designed research, Analyzed data, Edited manuscript
D.S.R.: Designed research, Analyzed data, Wrote manuscript, Secured Funding, Project leader

ABSTRACT

The RNA-binding protein IGF2BP3 is an oncofetal protein overexpressed in B-acute lymphoblastic leukemia and is critical for leukemogenesis in experimental models. With cancer-specific expression, functional dispensability for normal development, and an unleveraged pro-oncogenic function in mRNA homeostasis, IGF2BP3 represents an excellent target. With no small molecule inhibitors of IGF2BP3 in clinical use, we undertook an effort to identify new IGF2BP3 inhibitors using biochemical methods. A biochemical screen, followed by a cell-based counter screen, led to the identification of compounds with protein-RNA interaction inhibition and leukemic cell growth-inhibitory activity. One of these compounds, designated I3IN-002, shows consistent cell growth-inhibitory activity, altered cell cycle and increased apoptosis in multiple leukemia cell lines, and is the most potent inhibitor of IGF2BP3 reported to date. I3IN-002 was tolerated in mice when administered intraperitoneally and showed potent anti-leukemic activity in a syngeneic transplantation model of MLL-Af4 leukemia. I3IN-002 inhibits the function of IGF2BP3, disrupting in situ binding of IGF2BP3 to target mRNAs, and altering IGF2BP3-dependent gene expression regulation. Furthermore, cell-free and cellular thermal shift assays as well as drug affinity responsive target stability assays support on target activity of I3IN-002 for IGF2BP3. Thus, the identification of I3IN-002 paves the way for the discovery of potent and selective small molecule inhibitors of IGF2BP3.

INTRODUCTION

RNA binding proteins (RBPs) are important players in post-transcriptional gene regulation, and many show cancer-specific expression and may regulate oncogenesis via diverse mechanisms(1-5). The RNA binding protein IGF2BP3 was initially discovered as a factor overexpressed in pancreatic cancer and one of three homologous proteins (IGF2BP1-3) that bound to the 5'-untranslated region of the IGF2 mRNA(1). Since its original description, a large body of work has congruently demonstrated its role as an oncogenic protein in a number of different cancers, and that IGF2BP3 binds to the 3'UTR of mRNA(2). In acute leukemia, we and others initially identified IGF2BP3 as an upregulated RBP in MLL-translocated B-ALL(3, 4). IGF2BP3 is transcriptionally induced by MLL-AF4, and overexpression of IGF2BP3 in bone marrow led to hyperproliferation in hematopoietic stem and progenitor cells in mice(5). Moreover, deletion of *Igf2bp3* in vivo significantly limited leukemia development and increased leukemia-free survival(4, 6). At baseline, the *Igf2bp3* knockout mouse did not show any overt phenotypes, suggesting that it is dispensable for normal development and homeostasis in the adult. Together these studies established IGF2BP3 as an oncogenic target in acute leukemia.

To investigate the molecular mechanisms of IGF2BP3's action, we previously undertook eCLIP-seq, a technique designed to globally detect RNA molecules bound by IGF2BP3 in conjunction with differential expression analyses in cells that were depleted for IGF2BP3. These analyses revealed that IGF2BP3 most commonly binds to the 3'UTR of mRNA transcripts. The regulated mRNA transcripts included numerous downregulated oncogenes such as *HOXA9*, *CDK6* and *MYC(4, 7)*. Determinants of IGF2BP3-RNA binding include not only primary sequence but also epitranscriptomic modification of target mRNAs with N6-methyladenosine (m^6A) and spacing between short recognition sequences(6, 8-10). Importantly, deletion of the RNA-binding domains of IGF2BP3 abrogated stabilization of these transcripts, and reversed IGF2BP3-driven

pre-leukemic disease in vivo(11). Together these data suggest that IGF2BP3's binding to specific mRNAs is central to its role in promoting oncogenesis in the hematopoietic system.

RBPs were previously under-represented in targeted therapy approaches due to their presumed "undruggable" status, recent efforts have uncovered small molecules targeting RBPs, including the IGF2BP family(4, 12). With the oncogenic role of IGF2BP3 established by not only our studies but also from numerous other studies in literature, we sought to identify a small molecule inhibitor of the protein. To this end, we developed and validated a time-resolved Förster resonance energy transfer (TR-FRET) assay, using purified IGF2BP3 protein and a synthetic m^6A-modified target RNA molecule to measure binding. A library of small molecule compounds was applied to this assay, with resultant hit compounds being re-confirmed in TR-FRET assays and counter screened in cell-based assays. Confirmatory studies demonstrate activity in several leukemia cell lines with IGF2BP3 overexpression showed inhibition of cell growth and cell cycle progression, and increased apoptosis. One of these hit compounds, referred to here as I3IN-002, shows activity against leukemic initiating cells in vitro, and has anti-leukemic activity in vivo. I3IN-002 directly interferes with the function of IGF2BP3, as assessed by gene expression analyses and RNA immunoprecipitation experiments that measure IGF2BP3-dependent gene expression and IGF2BP3-mRNA binding. Furthermore, cellular thermal shift assays, cell-free thermal shift assay (TSA), and drug affinity responsive target stability (DARTS) support on-target activity for I3IN-002. I3IN-002 may prove useful as a tool compound in future biochemical studies involving IGF2BP3 and may also enable the development of novel therapeutics for the treatment of leukemia and other hematologic cancers.

METHODS

A complete description of methods can be found in Supplementary Information.

Cell lines and cell culture

All cell lines were maintained in standard conditions in an incubator at 37 °C and 5% CO_2. Human B-ALL cell lines, RS4;11 (ATCC CRL-1873), NALM6 (ATCC CRL-3273), SEM (DMZ-ACC 546), PER785 , REH (ATCC CRL-8286), OCI-AML 8227 and KASUMI-2 (DSMZ ACC 526), and immortalized MLL-Af4 transformed murine HSPCs were cultured as previously described(6). A full listing of reagents is provided in **Supp. Table 1**.

Antibodies. Antibodies were used for Western blotting, FACS, and immunoprecipitation experiments as described(4, 13, 14). A list of antibodies is provided in **Supp. Table 2.**

Protein Purification and High throughput assays.

IGF2BP3-GFP-Flag over-expression plasmid was constructed by fusing full length IGF2BP3 coding sequence (CDS) with GFP CDS and Flag CDS and cloned in pCDNA 3.0 vector. Protein was purified using standard methods and anti-Flag based affinity purification. Purified protein was added to pre-incubated Streptavidin-terbium plus biotinylated m6A-labeled RNA oligonucleotide (**Supp. Table 3**). The plate was incubated for 1 h at RT for binding and read on EnVision microplate reader (Perkin Elmer) with a dual PMT configuration using a 340 nm excitation and a dual emission mirror block with a 495 nm emission filter for Terbium fluorescence (W1 channel) and a 525 nm emission filter for GFP fluorescence (W2 channel). The assay was miniaturized to 10uL in 384-well plates and an in-house compound deck library at the UCLA MSSR was applied to the assay. Data analysis was performed as described in Supplementary Methods.

Counter-Screen and Cell-based Assays.

Wild-type and IGF2BP3-deleted SEM cell lines(6) were treated with compound, grown for 4 days under normal growth conditions, and assayed for cell growth in 384-well plates with CellTiter-Glo, a luminescence-based reagent described previously(6, 13, 14). Following identification of lead compounds, further measurements of apoptosis, cell cycle and proliferation were performed as we have previously described(6, 13, 14).

Compound Synthesis. Briefly, organic synthesis was performed utilizing commercially available fragments and a custom in-house strategy allowing for the design of the original compound and future analogs. Full description is provided in the Supplementary Methods.

Assays to define on-target activity.

A cellular thermal shift assay was performed on SEM cells treated with the test compound, based on published protocols with minor modifications described in the Supplementary Methods. The thermal shift assay with purified protein, and Drug Affinity responsive target stability assays were performed as previously described(15, 16). Lastly, RNA-sequencing to define differential gene expression, as well as RNA immunoprecipitation followed by sequencing (RIP-seq) were performed using standard methods(4, 17). RNA sequencing data has been deposited to the NCBI Short read archive with accession numbers PRJNA1333638 and PRJNA1336320.

Animal Experiments

For in vivo studies, C57BL/6J, B6.SJL-*Ptprc*^{a} *Pepc*^{b,}/BoyJ (B6 CD45.1), and B6J.129(Cg)-Gt(ROSA)26Sor$^{tm1.1(CAG-cas9_{*,}-EGFP)Fezh/J}$ (Cas9-GFP, BL/6J) were procured from The Jackson Laboratory. Preliminary toxicity studies were carried out to identify issues with small molecule delivery in non-transplanted mice. Primary murine leukemia cells (WT and Igf2bp3 KO)

prepared as previously described(14), were transplanted into busulfan-conditioned recipients. I3IN-002 was delivered intraperitoneally, three times a week for three weeks. Once the peripheral blood engraftment reached >20% at 4 weeks, the experiment was terminated and tissues were harvested to be analyzed by FACS, histology and RT-qPCR. A separate experiment examined overall and leukemia free survival. All of the animal experiments received Institutional Animal Research Committee approval at UCLA.

RESULTS

Disruptors of protein-RNA interactions are identified via biochemical screening.

To identify putative inhibitors of IGF2BP3 (I3), we designed and validated a time-resolved Förster resonance energy transfer (TR-FRET) assay, based on binding of a GFP-tagged I3 (I3-GFP) to a biotinylated RNA oligonucleotide carrying an m^6A modification (**Fig. 1a**). Small molecules that interfere with this interaction will lead to a loss of signal transfer, and subsequently decreased GFP fluorescence. For this assay, we generated a carboxy-terminal GFP- and FLAG-tagged IGF2BP3 protein-encoding mammalian expression vector (I3-GFP-F), cloned into pcDNA3.1 (**Supp. Fig. 1a**). We confirmed a functional fusion protein based on bright fluorescence following transfection and recognition with anti-IGF2BP3 antibodies (**Supp. Fig. 1b**). The protein was purified by elution from fractions 3-11 on an anti-FLAG column (**Supp. Fig. 1c**) and subsequently concentrated and quantitated by Coomassie staining (**Supp. Fig. 1d**). Functionality of the protein was confirmed by RNA immunoprecipitation of target mRNAs following incubation of purified protein with cell extracts and pulldown with anti-FLAG (**Supp. Fig. 1e-g**). Following purification and confirmation of RNA-binding activity, we confirmed that GFP fluorescence in the TR-FRET assay required the presence of all components (i.e., I3-GFP, biotinylated mRNA, and Terbium, **Fig. 1b**). The assay demonstrated saturation of the GFP fluorescence signal at approximately 50 nM of I3-GFP-F and 25 nM RNA oligonucleotide **(Fig. 1c and Supp. Fig. 1h)**. Next, we evaluated assay reproducibility across multiple experiments

performed across multiple days, finding excellent concordance in GFP fluorescence and Z'-values (**Supp. Fig. 1i-j**).

To adapt the assay to high throughput screening, we first successfully miniaturized the assay to 10 µL, while maintaining σ+ <20% and Z'>0.5, with highly reproducible GFP fluorescence (**Supp. Fig. 1k**). Following this validation, a high throughput screen of 196,567 compounds was completed in two stages, a preliminary screen, and a full-scale screen. We were able to successfully complete the screen: across 617 plates that were analyzed for this assay, a representative plate map is shown with and without hits (**Supp. Fig. 2a**). From the analysis, we achieved >99% of plates that showed standard deviation <20% and 95% of plates showed a Z' score greater than 0.5 (**Supp. Fig. 2b** and **Fig. 1d**). Plates that showed a low Z'-score were excluded from downstream hit confirmation. To define hits, we leveraged the preliminary screen to increase the specificity of hit definition (**Supp. Fig. 2 c**). Using only the primary criterion, defined as |Ratio Z|>3 (where Ratio is the ratio of terbium fluorescence/GFP fluorescence), we obtained a hit rate of 1.33% in the preliminary screen, and 1.73% in the full-scale screen (**Fig. 1e**). Using a secondary criterion, where Terbium fluorescence ("W1") was within one standard deviation of the mean for the plate (i.e., |W1 Z|<1), this reduced the hit rate to 0.94% and 0.19% in preliminary and full-scale screens, respectively (**Fig. 1e**). The reduced hit rate in the full-scale screen therefore is most likely due to increased variability in terbium fluorescence. Further refinements of hits, by an alternate secondary criterion definition (mean and standard deviation calculated for the experimental run, rather than the plate) and manual curation of the data when irregularities were observed, led to an initial, high-stringency list of 417 compounds that were further analyzed. Of the 417 hits out of 186,978 evaluable compounds, 29 contained a core structure with an indolyltriazine group (**Fig. 1f**). Remarkably, the library only contained 174 total compounds with the general structure depicted in **Fig. 1f**, representing ~74-fold enrichment for

these compounds, a highly statistically significant result (**Fig. 1g;** $p<0.0001$; Fisher's exact test). Together, our results identify a number of small molecules with in vitro activity against the RNA binding activity of IGF2BP3.

Cell-based counter screen identifies molecules with anti-leukemic activity.

To further characterize the hits identified from the screen, we first performed a confirmatory TR-FRET assay, with two experiments consisting of three replicates each. Concordant TR-FRET findings were characterized as Tier 1, 2 and 3, when findings were reproduced in 2/2, 1/2, or 0/2 experiments respectively. 89.3% (371/417) of hit compounds and 93.1% (27/29) of indolyltriazine compounds were Tier 1 or Tier 2 hits, respectively (**Supp. Fig. 2d**). To further examine these confirmed hits, we turned to a cell-based assay (**Fig. 2a**). Here, we reasoned that a compound that was specific for IGF2BP3 would only show activity in SEM cell lines that contained intact, increased expression of the protein (SEM-WT), with reduced activity in cell lines with experimental deletion via CRISPR-Cas9 (SEM-I3KO). Cells were treated with compound, grown for 4 days under normal growth conditions, and assayed for cell growth with CellTiter-Glo, a luminescence-based reagent described previously(6, 13, 14). Fold change from control (i.e., no compound treated wells) was plotted for SEM-WT versus SEM-I3KO. Remarkably, there were compounds that showed enhanced reduction of cell growth in SEM-WT, as opposed to SEM-I3KO (**Fig. 2b**). Using the cutoff (Growth Ratio<0.7 OR WT Growth<0.7), we identified 16 compounds . We then chose three promising compounds, designated **1**, **2** and **3** here, and tested them across a range of concentrations on SEM cells (**Fig. 2c-e**). Of these, **2** and **3**, which we later designated as **I3IN-002** and **I3IN-003**, showed differential activity in the two cell lines, with **2** showing a promising IC_{50} of ~2 μM in wild-type SEM-cells (**Fig. 2d**). A summary of the compound screening, validation and selection of the hit compounds is depicted in **Supp. Fig. 2e**.

I3IN-002 inhibits cell proliferation and cell cycle progression and promotes apoptosis.

To enable further biological evaluation, we sought to prepare **I3IN-002** in high purity and in larger quantities compared to what was available commercially. Moreover, chemical characterization data for **I3IN-002** was not identified in the literature. To access **I3IN-002**, we performed the synthetic route shown in (**Fig. 3a**). First, isatin **4** was treated with thiosemicarbazide (**5**) and potassium carbonate in methanol at ambient temperature to give hydrazone formation. The hydrazone intermediate was subjected to potassium carbonate in water at reflux to give triazinoindolothione **6**(18). In the next step, intermediate **6** was treated with alkyl chloride **7** in the presence of potassium carbonate in DMSO(19). This delivered **I3IN-002**, which was isolated as a powder. The purity of **I3IN-002** was deemed to be >97% by both quantitative ^{1}H NMR and HPLC analysis.

To characterize the activity of I3IN-002, we tested the compound in a number of leukemia models, including SEM, RS4;11, PER 785, KASUMI-2, NALM6, REH, and MLL-Af4 Lin- cells after studying the baseline expression of IGF2BP3 in these cells (**Supp. Fig. 3a**). IC50 experiments performed on these cell lines showed the compound is more potent in B-ALL cell lines with MLL-AF4 translocation, with lower IC50 values compared to other B-ALL cell lines (**Fig. 3b**). Treatment with a single dose of I3IN-002 resulted in a dose-dependent growth inhibition of SEM, RS4;11 Lin-MLL-Af4 and MV4;11 cells at the concentrations tested in our assays (**Fig. 3c-e and Supp. Fig. 3b**). Moreover, cell cycle profiling using propidium iodide in both SEM and RS4;11 cells showed an increase in sub-G0 cells (**Fig. 4a and Supp. Fig. 3c-3d**); changes in other phases of the cell cycle were not as consistent. This may be in part, because in SEM cells the G2-M transition genes such as CDK1 and CCNB2, which are also regulated by IGF2BP3 , were downregulated due to compound treatment (**Supp. Fig. 3e-3f**).

Next, we analyzed the effect of I3IN-002 on cellular apoptosis. These studies showed an increase in apoptosis, as detected by Caspase 3/7 activity in both SEM and RS4;11 cells (**Fig. 4b-4c**). Treatment also led to a numerically small but statistically significant increase in Annexin V+ cells as well as in necrotic cells (Annexin V+ and propidium iodide+) in both SEM and RS4;11 cells (**Fig. 4d and Supp. Fig. 3g-h**). Together, these studies indicate that I3IN-002 impacts cell growth, cell cycle, and apoptosis in a variety of target cell lines, with an enhanced growth inhibitory effect in MLL-AF4-driven leukemia.

Reduction of leukemia-initiating cells and leukemia engraftment in vivo by I3IN-002.

Given our previous work showing that genetic ablation of *Igf2bp3* led to a reduction in leukemia initiating cells, we next assayed whether I3IN-002 caused an effect on plating efficiency in methylcellulose colony formation assays. Similar to genetic knockout, I3IN-002 treatment led to a reduction in total colony counts in a dose-dependent manner and a reduction in the fraction of cells that showed expression of CD34 and c-kit (**Fig. 4e-f and Supp. Fig. 3i**). We also observed a reduction in the CD34+CD38+ fraction (thought to correspond to leukemic stem cells (20) in OCI-AML8227 cells (**Supp. Fig. 3j-k**). With these findings, we next evaluated the compound in vivo.

For in vivo experiments, mice syngeneically transplanted with the Lin-MLL-Af4 cells (either WT or I3KO, **Supp. Fig. 4a**) were injected intraperitoneally with I3IN-002 or vehicle control using the schedule indicated (**Fig. 5a**). This model demonstrates a rapid and lethal leukemia that primarily involves the bone marrow and spleen, with lesser involvement of the peripheral blood. Here, we used the genetic deletion of *Igf2bp3* as a positive control for the predicted effect of IGF2BP3 inhibition, as genetic ablation prevents leukemia development(13, 14). Upon harvest at 4 weeks post-transplant, WT-transplanted mice that received I3IN-002 showed significantly reduced

spleen size and weight compared to vehicle treated control mice, but larger than I3KO-transplanted mice (**Fig. 5b and 5c**). FACS analysis revealed that in vivo treatment reduced the number of CD34+ c-kit+ cells in both the spleen and the bone marrow (**Fig. 5d and Supp. Fig. 4b**). In the spleen, leukemic engraftment (**Fig. 5e** and **Supp. Fig. 4c**) and the proportion of CD11b+ cells (**Supp. Fig. 4d-e)**) and of CD34+ Sca1- cells were reduced significantly (**Supp. Fig. 4f**). In the bone marrow, overall leukemic engraftment was not different following I3IN-002 treatment compared to vehicle (**Supp. Fig. 4g**), but significant reductions in CD11b+ and CD34+ Sca1- cells were noted (**Supp. 4h-4i**) Histologically, we observed lower levels of leukemic engraftment in the liver (compare cellular area next to arrow) and reduced architectural distortion and lower leukemic engraftment in the spleen (compare size of dotted areas and intervening cellularity) in I3IN-002 treated mice, and as expected in I3KO (**Fig. 5f**). Similar reductions in engraftment were also noted in lung and kidney (**Supp. Fig. 4j**). Notably, we found significant improvement in overall survival following I3IN-002 treatment in a separate set of endpoint experiments (**Fig. 5g**). Together, these data indicate a significant effect of I3IN-002 on leukemic burden, corresponding with a reduction in the leukemic initiating cell fraction, thus inhibiting leukemogenesis and extending survival.

I3IN-002 inhibits IGF2BP3-dependent gene expression changes.

Prior work by our group and others(14) has shown that IGF2BP3 functions in post-transcriptional gene regulation by binding to mRNA molecules and regulating their expression. To understand the downstream consequences of IGF2BP3 inhibition, we performed RNA-seq of DMSO-treated, I3IN-002-treated and I3KO SEM cells (**Supp. Fig. 5a**). These studies resulted in the identification of differentially expressed genes between SEM-WT and SEM-I3KO (n=319 genes) as well as between SEM-WT and SEM-WT-I3IN-002 treated cells (n=226 genes). Volcano plots demonstrate that the overall changes in gene expression were more pronounced

in the genetic knockout of IGF2BP3 compared to I3IN-002 treated cells (**Fig. 6a**). Remarkably, 63 genes were common between the two datasets, which represents a highly significant overlap (nearly 28% of genes regulated by I3IN-002-treatment; Hypergeometric test, p-value $<10^{-16}$; **Fig. 6b**; see also **Supp. Fig. 5b**). Gene set enrichment analyses of the overlap genes between I3KO and I3IN-002 treated cells showed many pathways that we have previously associated with IGF2BP3 function, including response to oxidative stress, cell activation, cellular response to cytokine stimulus, and neutrophil degranulation (**Fig. 6c**). By RT-qPCR, we noted concordant changes in mRNA levels of *P4HA1*, *BTG2*, *KDM3A*, *BNIP3L*, *TGFBR2*, as well as IGF2BP3 targets *BCL2*, *CDK6, MYC*, and *HOXA9* (4, 6) (**Fig. 6d-i and Supp. Fig. 5c-e**). Next, to examine these findings at the protein level, we performed Western Blotting for three of the proteins encoded by the altered mRNAs, finding decrease in the levels of P4HA1, BTG2, and KDM3A with both I3IN-002 treatment and I3KO (**Fig. 6j**). These protein-level changes were also observed for previously identified targets of IGF2BP3, CDK6 and BCL2 (**Fig. 6k**). Paralleling the findings in cell culture, *Cdk6, Myc, Hoxa9, Kdm3a, Bnip3l* and *Bcl2* mRNAs, were downregulated in spleen samples from mice treated with I3IN-002, based on RT-qPCR (**Supp. Fig. 5f-5k**).

I3IN-002 inhibits the molecular function of IGF2BP3 in gene regulation.

To test how I3IN-002 impacts IGF2BP3 function, we also performed RNA immunoprecipitation (RIP) following treatment with I3IN-002 (**Fig. 7a**). Following confirmation of IGF2BP3 pull-down after immunoprecipitation, we subjected the co-immunoprecipitated RNA to high-throughput sequencing (RIP-seq) (17). The analysis allowed us to identify mRNAs that were significantly enriched in the immunoprecipitated fraction (padj<0.01), for which we calculated enrichment ratios (fold change of immunoprecipitated RNA versus input RNA). Genes found to be enriched in the control sample (DMSO) were designated as I3 RIP targets. Comparison of these targets

with previously identified targets of IGF2BP3 determined by enhanced cross-link-immunoprecipitation and RNA sequencing (eCLIP-seq) in these same cells showed a highly statistically significant overlap (489/772 I3eCLIP-seq targets also seen by RIP-seq; Hypergeometric test $p<10^{-16}$; **Fig. 7b**). With confidence that RIP-seq had identified known I3 targets, we proceeded to compare the enrichment ratios between the two conditions, finding that the overall degree of up- and down-regulated transcripts were roughly the same. However, we noted that the more highly enriched transcripts, as well as those with a higher difference in enrichment ratios between conditions, showed a skewing towards decreased enrichment in the I3IN-002-treated samples. When we limited the analysis to those transcripts with a difference in enrichment ratios greater than 1 and that were also targets identified by eCLIP-seq, we found that these were highly enriched for transcripts whose interactions with I3 were inhibited (**Fig. 7c**). Using individual qPCRs, we found that four mRNAs that we have previously found to be associated with IGF2BP3, *BCL2*, *CDK6, MYC,* and *HOXA9*, as well as genes such as PAICS and HMGA1 identified from the RIP-seq, were decreased in the immunoprecipitate following IGF2BP3 pulldown (**Fig. 7d** and **Supp. Fig. 6a-d**). Downstream of binding, IGF2BP3 modulates protein expression of its target transcripts, upregulating the expression of oncogenes such as *BCL2*, *CDK6, HOXA9*(4, 14). Using a 3'UTR-luciferase reporter assay, we found that I3IN-002 inhibits protein expression linked to target 3'UTRs of *CDK6, BNIP3L,* and *BCL2* suggesting a concordant functional effect of compound treatment (**Fig. 7e**). Next, to assess *in situ* binding of I3IN-002 to IGF2BP3, we performed a cellular thermal shift assay, finding a difference in thermal stability, as assessed by Western blot and quantitation **(Fig. 7f and Supp. Fig. 6e)**. Direct interaction of I3IN-002 with IGF2BP3 was confirmed using orthogonal methods. Thermal shift assay (TSA) using purified full length IGF2BP3 demonstrated stabilization of IGF2BP3 with compound (**Fig. 7g and Supp. Fig. 6f**), while DARTS demonstrated I3IN-002 dependent inhibition of protease mediated degradation of IGF2BP3 (**Supp. Fig. 6g**). Together, these

findings support a mechanism wherein I3IN-002 is impacting the function of IGF2BP3 in its critical role as a post-transcriptional regulator of mRNA homeostasis.

DISCUSSION

The RNA-binding protein IGF2BP3 is a potent oncofetal protein, as demonstrated by our work and that of many others. In this manuscript, we describe the successful completion of a high-throughput biochemical screening assay that utilizes the RNA-binding function of IGF2BP3 as the discriminant for small molecule activity. Combining the biochemical screen with a cell-based assay to detect IGF2BP3-dependent effects on leukemic cell growth and survival, we identified 16 compounds that are likely to have activity in an IGF2BP3-specific manner. The first of these compounds to be confirmed is I3IN-002, which shows an IC_{50} of approximately 2 μM in initial assays. Specifically, I3IN-002 inhibited cell growth, impacted cell cycle progression of treated cells, and increased apoptosis. I3IN-002 inhibited leukemia-initiating cells and showed in vivo anti-leukemic activity. Furthermore, I3IN-002 impacted global gene expression in a manner similar to genetic deletion of IGF2BP3. CETSA, TSA, DARTS and RNA immunoprecipitation experiments supported on-target activity against IGF2BP3.

RNA-binding proteins have recently been appreciated as biologically and clinically significant regulators of gene expression(12, 21-23). This recognition has led to a growing effort to target RNA binding proteins, but challenges exist(12, 24). First, many cancer-associated RNA binding proteins are also required for normal homeostasis(25) and hence, targeting these proteins might engender significant toxicity. The IGF2BP family of proteins has emerged as cancer-specific or cancer-enriched proteins, and IGF2BP3 is an oncofetal protein, making this an attractive cancer target. Second, while oligonucleotide-based therapies hold great promise, targeting of many tissues, including cancer, remains a major challenge in the field. Hence, small molecule therapeutics hold many advantages, including delivery and bioavailability, with the

development of reproducible and straightforward synthesis methods allowing for future large-scale manufacturing and distribution. Our efforts here have resulted in some of the first small molecules identified by empirical, experimental approaches to target IGF2BP3. Moreover, the molecule identified here, I3IN-002, is effective at inhibiting the protein-RNA interaction, as measured by multiple reporter assays. We suggest that this parameter may be a critical and useful measure of efficacy of small molecules for targeting post-transcriptional regulation.

In recent years, several small molecules have been reported to inhibit the IGF2BP family of proteins. Regulators of expression include an isocorydine derivative, 8-amino-ICD, which was reported to target hepatocellular carcinoma and decrease IGF2BP3 expression at an EC_{50} of 20 μM or greater(26). In non-small cell lung cancer, isoliquiritigenin is also able to down-regulate IGF2BP3 expression in a dose-dependent manner(27). Most recently, a virtual screening approach identified AE-848 as an inhibitor of IGF2BP3 with an IC_{50} of ~10- 40μM in ovarian cancer(28). Other IGF2BP proteins have been reported to be targeted by small molecules: BTYNB targets IGF2BP1 (IC_{50} of 5-10 μM); JX1 targets IGF2BP2 ($IC_{50\ of}$ 10- 20 μM) in acute T-lymphoblastic leukemia, and CWI1-2 also targets IGF2BP2 (sub-micromolar IC_{50} in AML cell lines)(29-31). Our discoveries here indicate that I3IN-002 is the most potent inhibitor of IGF2BP3 reported to date, and the first in hematologic malignancy, and strongly support its role in altering oncogenic post-transcriptional gene regulation, providing the impetus for further drug discovery efforts.

Biologically active small molecules containing indolyltriazine cores possess potent and selective activity across a variety of indications. Other anti-cancer compounds containing the motif include an inhibitor of tyrosine phosphatase SHP-2(32), and a commercially available tool compound, Inauhzin, which acts as a SIRT-1 inhibitor(33). Further, this motif has also been

found in antibiotics, α-glucosidase inhibitors, and targeted P-glycoprotein inhibitors, amongst other classes of biologically relevant molecules(18, 34-36). Notably, many of these compounds are demonstrated to be highly selective. This relatively diverse set of targets is consistent with our findings that small changes in the structure can markedly alter the bioactivity of the indolyltriazine in acute leukemia (i.e., only 2 out of 29 TR-FRET-active indolyltriazine compounds tested showed bioactivity). In other words, the specificity of the compounds may be highly malleable with chemical modifications of the side chains. Our initial efforts indicate that I3IN-002 can be readily synthesized using widely commercially available component molecules. This information should enable future efforts to develop compound analogs of I3IN-002 that display selective binding to IGF2BP3, without off-target effects. Importantly, while the indolyltriazine core is seemingly privileged with respect to bioactivity, it is not found in any commercially available drugs to date.

It is also of interest to note that we recently showed that IGF2BP3 genetic ablation was additive with menin inhibition in MLL-AF4 leukemia(14). While outside the scope of this report, compounds generated here could therefore be useful in combinatorial therapeutic approaches with menin inhibition, inhibiting leukemia at the transcriptional and post-transcriptional levels. In addition, IGF2BP3 targets include a number of key oncogenic proteins, which are themselves the targets of advanced small molecule development programs. For example, CDK6 is a direct target of IGF2BP3 that is upregulated by the latter's activity, and anti-CDK4/6 inhibitors have been developed as potent agents in cancer therapy, for example, in breast cancer(37). BCL2 is also a direct target of IGF2BP3, and the BCL2 inhibitor Venetoclax has shown activity in a number of hematologic malignancies, including B-ALL and AML. Other IGF2BP3 targets, such as MYC, which have long been elusive as drug targets, are also now being actively pursued with small molecule approaches(38). Hence, our development of IGF2BP3 small molecule

inhibitors could be especially important in future combinatorial therapy approaches, which is an important future direction for our work.

While this work contains important advances, showing that disrupting IGF2BP3-RNA binding can be the basis of a therapeutic approach in selected hematologic malignancies, we acknowledge that there are areas for important future work. In vitro studies of binding affinities have yet to be completed, due to difficulties in purifying full-length protein in quantities sufficient for detailed biochemical analyses. We believe this is because the protein may be prone to liquid-liquid phase separation, and prior work has focused on individual domains within the protein, yielding crystal structures of protein subdomains only(39-42). Moreover, pharmacological parameters of this compound and it's derivatives will require optimization. Thus, future directions will involve analog synthesis and biochemical evaluation to ultimately improve and validate selective binding to IGF2BP3, while also optimizing drug-like properties.

Overall, our study has led to the discovery and validation of I3IN-002, a small molecule that inhibits IGF2BP3-RNA interactions. While our work has thus far focused on the role of IGF2BP3 in acute leukemia, it is known that IGF2BP3 is overexpressed in a range of B-cell malignancies, including diffuse large B-cell lymphoma, Burkitt lymphoma and others(43-45). Moreover, it is estimated that up to 15% of all human cancers overexpress IGF2BP3, including both hematologic and non-hematologic malignancies, with high levels correlated with aggressive tumor behavior by expression and functional analyses(3, 21, 46-50). Consistent with the notion of being an oncofetal protein, our work has determined that IGF2BP3 appears to be largely dispensable in homeostatic development(6), providing a significant therapeutic window for targeting. It should be noted that IGF2BP3 expression is quite variable within different types of cancer, and hence, future indications will need to be carefully defined. We speculate that IGF2BP3 expression could be evaluated in different cancer types by widely available techniques

such as immunohistochemistry, and compounds such as I3IN-002 or future derivatives could be administered as a precision medicine intervention in carefully selected patients. Hence, I3IN-002 serves as a promising lead compound for future drug discovery efforts aimed at identifying selective inhibitors of IGF2BP3, particularly for the treatment of acute leukemia.

References

1. Müeller-Pillasch F, Lacher U, Wallrapp C, et al. Cloning of a gene highly overexpressed in cancer coding for a novel KH-domain containing protein. Oncogene. 1997;14(22):2729-2733.
2. Nielsen J, Christiansen J, Lykke-Andersen J, Johnsen AH, Wewer UM, Nielsen FC. A family of insulin-like growth factor II mRNA-binding proteins represses translation in late development. Mol Cell Biol. 1999;19(2):1262-1270.
3. Mancarella C, Scotlandi K. IGF2BP3 From Physiology to Cancer: Novel Discoveries, Unsolved Issues, and Future Perspectives. Front Cell Dev Biol. 2020;7:363.
4. Palanichamy JK, Tran TM, Howard JM, et al. RNA-binding protein IGF2BP3 targeting of oncogenic transcripts promotes hematopoietic progenitor proliferation. J Clin Invest. 2016;126(4):1495-1511.
5. Stoskus M, Gineikiene E, Valceckiene V, Valatkaite B, Pileckyte R, Griskevicius L. Identification of characteristic IGF2BP expression patterns in distinct B-ALL entities. Blood Cells Mol Dis. 2011;46(4):321-216.
6. Tran TM, Philipp J, Bassi JS, et al. The RNA-binding protein IGF2BP3 is critical for MLL-AF4-mediated leukemogenesis. Leukemia. 2022;36(1):68-79.
7. Lin S, Luo RT, Ptasinska A, et al. Instructive Role of MLL-Fusion Proteins Revealed by a Model of t(4;11) Pro-B Acute Lymphoblastic Leukemia. Cancer Cell. 2016;30(5):737-749.
8. Yang Z, Wang T, Wu D, Min Z, Tan J, Yu B. RNA N6-methyladenosine reader IGF2BP3 regulates cell cycle and angiogenesis in colon cancer. J Exp Clin Cancer Res. 2020;39(1):203.
9. Huang H, Weng H, Sun W, et al. Recognition of RNA N(6)-methyladenosine by IGF2BP proteins enhances mRNA stability and translation. Nat Cell Biol. 2018;20(3):285-295.
10. Ren F, Lin Q, Gong G, et al. Igf2bp3 maintains maternal RNA stability and ensures early embryo development in zebrafish. Commun Biol. 2020;3(1):94.
11. Gu Y, Niu S, Wang Y, et al. DMDRMR-Mediated Regulation of m(6)A-Modified CDK4 by m(6)A Reader IGF2BP3 Drives ccRCC Progression. Cancer Res. 2021;81(4):923-934.
12. Elcheva IA, Spiegelman VS. Targeting RNA-binding proteins in acute and chronic leukemia. Leukemia. 2021;35(2):360-376.
13. Jaiswal AK, Truong H, Tran TM, et al. Focused CRISPR-Cas9 genetic screening reveals USO1 as a vulnerability in B-cell acute lymphoblastic leukemia. Sci Rep. 2021;11(1):13158.
14. Lin TL, Jaiswal AK, Ritter AJ, et al. Targeting IGF2BP3 enhances antileukemic effects of menin-MLL inhibition in MLL-AF4 leukemia. Blood Adv. 2024;8(2):261-275.
15. Jafari R, Almqvist H, Axelsson H, et al. The cellular thermal shift assay for evaluating drug target interactions in cells. Nat Protoc. 2014;9(9):2100-2122.
16. Pai MY, Lomenick B, Hwang H, et al. Drug affinity responsive target stability (DARTS) for small-molecule target identification. Methods Mol Biol. 2015;1263:287-298.
17. Sharma G, Tran TM, Bansal I, et al. RNA binding protein IGF2BP1 synergizes with ETV6-RUNX1 to drive oncogenic signaling in B-cell Acute Lymphoblastic Leukemia. J Exp Clin Cancer Res. 2023;42(1):231.

18. Rahim F, Ullah K, Ullah H, et al. Triazinoindole analogs as potent inhibitors of alpha-glucosidase: synthesis, biological evaluation and molecular docking studies. Bioorg Chem. 2015;58:81-87.
19. Shelke SM, Bhosale SH. Synthesis, antidepressant evaluation and QSAR studies of novel 2-(5H-[1,2,4]triazino[5,6-b]indol-3-ylthio)-N-(substituted phenyl)acetamides. Bioorg Med Chem Lett. 2010;20(15):4661-4664.
20. Subedi A, Liu Q, Ayyathan DM, et al. Nicotinamide phosphoribosyltransferase inhibitors selectively induce apoptosis of AML stem cells by disrupting lipid homeostasis. Cell Stem Cell. 2021;28(10):1851-1867.e8.
21. Bell JL, Wachter K, Muhleck B, et al. Insulin-like growth factor 2 mRNA-binding proteins (IGF2BPs): post-transcriptional drivers of cancer progression? Cell Mol Life Sci. 2013;70(15):2657-2675.
22. Wang E, Lu SX, Pastore A, et al. Targeting an RNA-Binding Protein Network in Acute Myeloid Leukemia. Cancer Cell. 2019;35(3):369-384.e7.
23. Gebauer F, Schwarzl T, Valcarcel J, Hentze MW. RNA-binding proteins in human genetic disease. Nat Rev Genet. 2021;22(3):185-198.
24. Tran TM, Rao DS. RNA binding proteins in MLL-rearranged leukemia. Exp Hematol Oncol. 2022;11(1):80.
25. Jaiswal AK, Thaxton ML, Scherer GM, Sorrentino JP, Garg NK, Rao DS. Small molecule inhibition of RNA binding proteins in haematologic cancer. RNA Biol. 2024;21(1):1-14.
26. Li M, Zhang L, Ge C, et al. An isocorydine derivative (d-ICD) inhibits drug resistance by downregulating IGF2BP3 expression in hepatocellular carcinoma. Oncotarget. 2015;6(28):25149-25160.
27. Cui Y, Wu Y, Wang C, et al. Isoliquiritigenin inhibits non-small cell lung cancer progression via m(6)A/IGF2BP3-dependent TWIST1 mRNA stabilization. Phytomedicine. 2022;104:154299.
28. Shu C, Gu MH, Zeng C, et al. Small-molecule exhibits anti-tumor activity by targeting the RNA m(6)A reader IGF2BP3 in ovarian cancer. Am J Cancer Res. 2023;13(10):4888-4902.
29. Weng H, Huang F, Yu Z, et al. The m(6)A reader IGF2BP2 regulates glutamine metabolism and represents a therapeutic target in acute myeloid leukemia. Cancer Cell. 2022;40(12):1566-1582.e10.
30. Mahapatra L, Andruska N, Mao C, Le J, Shapiro DJ. A Novel IMP1 Inhibitor, BTYNB, Targets c-Myc and Inhibits Melanoma and Ovarian Cancer Cell Proliferation. Transl Oncol. 2017;10(5):818-827.
31. Feng P, Chen D, Wang X, et al. Inhibition of the m(6)A reader IGF2BP2 as a strategy against T-cell acute lymphoblastic leukemia. Leukemia. 2022;36(9):2180-2188.
32. Yu WM, Guvench O, Mackerell AD, Qu CK. Identification of small molecular weight inhibitors of Src homology 2 domain-containing tyrosine phosphatase 2 (SHP-2) via in silico database screening combined with experimental assay. J Med Chem. 2008;51(23):7396-7404.
33. Zhang Q, Zeng SX, Zhang Y, et al. A small molecule Inauhzin inhibits SIRT1 activity and suppresses tumour growth through activation of p53. EMBO Mol Med. 2012;4(4):298-312.

34. Garzan A, Willby MJ, Ngo HX, et al. Combating Enhanced Intracellular Survival (Eis)-Mediated Kanamycin Resistance of Mycobacterium tuberculosis by Novel Pyrrolo[1,5-a]pyrazine-Based Eis Inhibitors. ACS Infect Dis. 2017;3(4):302-309.
35. Li H, Liu J, Liu CF, et al. Design, Synthesis, and Biological Evaluation of Membrane-Active Bakuchiol Derivatives as Effective Broad-Spectrum Antibacterial Agents. J Med Chem. 2021;64(9):5603-5619.
36. Wise JG, Nanayakkara AK, Aljowni M, et al. Optimizing Targeted Inhibitors of P-Glycoprotein Using Computational and Structure-Guided Approaches. J Med Chem. 2019;62(23):10645-10663.
37. Wang X, Zhao S, Xin Q, Zhang Y, Wang K, Li M. Recent progress of CDK4/6 inhibitors' current practice in breast cancer. Cancer Gene Ther. 2024;31(9):1283-1291.
38. Boike L, Cioffi AG, Majewski FC, et al. Discovery of a Functional Covalent Ligand Targeting an Intrinsically Disordered Cysteine within MYC. Cell Chem Biol. 2021;28(1):4-13.e7.
39. Schneider T, Hung LH, Aziz M, et al. Combinatorial recognition of clustered RNA elements by the multidomain RNA-binding protein IMP3. Nat Commun. 2019;10(1):2266.
40. Li X, Guo W, Wen Y, et al. Structural basis for the RNA binding properties of mouse IGF2BP3. Structure. 2025;33(4):771-785.e3.
41. Jia M, Gut H, Chao JA. Structural basis of IMP3 RRM12 recognition of RNA. RNA. 2018;24(12):1659-1666.
42. Zeng WJ, Lu C, Shi Y, et al. Initiation of stress granule assembly by rapid clustering of IGF2BP proteins upon osmotic shock. Biochim Biophys Acta Mol Cell Res. 2020;1867(10):118795.
43. King RL, Pasha T, Roullet MR, Zhang PJ, Bagg A. IMP-3 is differentially expressed in normal and neoplastic lymphoid tissue. Hum Pathol. 2009;40(12):1699-1705.
44. Kosari F, Bakhshi T, Ameli F, Mokhtari M. The utility of IMP3 immunohistochemical staining in differentiating nodular lymphocyte predominant Hodgkin Lymphoma from T-Cell/Histiocyte-Rich large B-Cell lymphoma. BMC Cancer. 2022;22(1):1359.
45. Saka M, Fujimoto M, Mizoguchi K, et al. Insulin-like Growth Factor II mRNA-binding Protein 3 is a Highly Sensitive Marker for Intravascular Large B-cell Lymphoma: Immunohistochemical Analysis of 152 Pathology Specimens From 88 Patients. Am J Surg Pathol. 2024;48(6):671-680.
46. Lederer M, Bley N, Schleifer C, Huttelmaier S. The role of the oncofetal IGF2 mRNA-binding protein 3 (IGF2BP3) in cancer. Semin Cancer Biol. 2014;29:3-12.
47. Schaeffer DF, Owen DR, Lim HJ, et al. Insulin-like growth factor 2 mRNA binding protein 3 (IGF2BP3) overexpression in pancreatic ductal adenocarcinoma correlates with poor survival. BMC Cancer. 2010;10:59.
48. Kobel M, Xu H, Bourne PA, et al. IGF2BP3 (IMP3) expression is a marker of unfavorable prognosis in ovarian carcinoma of clear cell subtype. Mod Pathol. 2009;22(3):469-475.
49. Lochhead P, Imamura Y, Morikawa T, et al. Insulin-like growth factor 2 messenger RNA binding protein 3 (IGF2BP3) is a marker of unfavourable prognosis in colorectal cancer. Eur J Cancer. 2012;48(18):3405-3413.

50. Jonson L, Christiansen J, Hansen TVO, Vikesa J, Yamamoto Y, Nielsen FC. IMP3 RNP safe houses prevent miRNA-directed HMGA2 mRNA decay in cancer and development. Cell Rep. 2014;7(2):539-551.

FIGURE LEGENDS

Figure 1. Design and execution of a high throughput assay to identify small molecule inhibitors of IGF2BP3.

a. Schematic of assay. IGF2BP3-GFP fusion protein is bound to an m^6A-modified, biotinylated RNA oligonucleotide, which in turn is bound to Streptavidin Terbium (SA-Tb). Förster resonance energy transfer occurs when the protein and RNA are bound.

b. GFP Fluorescence (fold- change over control) plotted for different combinations of Streptavidin Terbium (SA-Tb), IGF2BP3-GFP (I3-GFP), m^6A-modified RNA (m^6A RNA) or unmethylated, biotinylated RNA (RNA).

c. GFP Fluorescence (arbitrary units) as a function of IGF2BP3-GFP protein concentration.

d. High throughput screening assay Z'-scores for control reactions across 600+ plates screening over 186,978 compounds.

e. Screening was conducted first with a limited set of compounds (preliminary screen) prior to a full-scale screen. Fluorescence ratios were calculated as W1/W2 where W1 is the Terbium fluorescence and W2 is the GFP fluorescence. Shown are the percentages of compounds satisfying a single criterion (i.e., Ratio Z) or two criteria (Ratio Z and W1 Z).

f. First "core structure" identified from the screen. The indolyltriazine substructure was conserved across multiple hits from screening in d and e.

g. Comparison of total number of hits in the library, versus hits amongst compounds containing the first core structure; Fisher's exact test, $p<0.0001$.

Figure 2. Identification of molecules with biochemical activity and IGF2BP3-dependent anti-proliferative properties.

a. Counter-screen strategy: SEM cells with (SEM-WT) and without IGF2BP3 (SEM-I3KO) are treated in a medium-throughput format with the small molecules identified from the biochemical screen.

b. Scatter plot examining the relationship between relative changes in cell growth, measured by CellTiterGlo and normalized to DMSO control, in SEM-WT (x-axis) and SEM-I3KO (y-axis). Compounds *1*, *2* and *3* (red-brown) were noted to have a preferential effect on SEM-WT and a lesser effect in SEM-I3KO. Cells were treated with 5 μM solutions of test compounds.

c-e. Structures of compounds *1*, *2* and *3* (top) and corresponding concentration dependent changes in cell growth rate (bottom) for the three compounds with favorable characteristics on screening. Growth rate was measured using CellTiterGlo and normalized to DMSO control in SEM-WT cell line.

Figure 3. I3IN-002 hampers cell growth in human and mouse leukemic cells.

a. Chemical synthesis of **I3IN-002**.

b. IC50 values of I3IN-002 on MLLr B-ALL and B-ALL cell lines.

c-e. Concentration-dependent alterations of cell growth curves over 4 days of cell culture with

I3IN-002 treatment, assessed by CellTiterGlo assay, and plotted as relative luminescence units (RLU). SEM (c), RS4;11 (d), and Lin-/MLL-Af4 (e) cells were assayed in this experiment. Data represent mean and standard error of the mean in 8 replicates.

Figure 4. I3IN-002 treatment causes cell cycle arrest and apoptosis in human and mouse leukemic cells.

a. Measurement of sub-G0 cells by propidium iodide staining in SEM and RS4;11 cells, respectively, following treatment with 5 μM I3IN-002 or DMSO. Data represents mean and

standard error of the mean of the calculated percentage of cells at each stage of cell cycle with 3 replicates.

b-c. Measurement of apoptosis induction, by Caspase 3/7 activity assay in SEM and RS4;11cells. Data represents mean and standard error of mean with 8 replicates.

d. Measurement of cell death by orthogonal method of Annexin V and propidium iodide staining in SEM and RS4;11 cells. Shown are the % of cells that are single or double positive for propidium iodide and Annexin V.

e. Quantitation of a leukemic stem-cell enriched population by assaying the CD34+ c-kit+ population following in vitro treatment of Lin-/MLL-Af4 cells in culture.

f. Measurement of colony formation in methylcellulose following treatment of a murine model of MLL-Af4 driven leukemia (14) with I3IN-002. Data represents the mean number of total colonies for each condition, with 3 replicates per condition. I3KO represents genetic knockout of IGF2BP3, which results in reduced colony formation

For Figures 3 and 4, statistical significance was evaluated by student's T-test, *$p<0.05$; **$p<0.01$; ***$p<0.001$; ****$p<0.0001$.

Figure 5. I3IN-002 inhibits leukemic growth in vivo.

a. Schematic of mouse experiment.

b. Gross pathology photographs of murine spleens from mice syngeneically transplanted with Lin-/MLL-Af4 cells. I3KO are genetic knockouts of IGF2BP3, which markedly reduced leukemic engraftment.

c. Splenic weights from treated mice, as indicated.

d. FACS staining for CD34 and c-kit in the spleen of treated mice, as indicated.

e. Quantification of overall leukemia engraftment in the spleen.

f. Histology of liver (top) and spleen (bottom) from treated mice, as indicated. Arrow indicates a leukemic infiltrate in the liver in the portal area. Dotted lines indicate splenic white pulp, with leukemic infiltrates in the red pulp (area outside the dotted lines). Hematoxylin and eosin staining, original magnification, 200X.

g. Kaplan-Meier survival curve shows effect of I3IN-002 injection on overall survival in syngeneic bone marrow transplant experiment.

Data in e-k represents one experiment composed of the following numbers of animals: Vehicle, n=8; I3IN-002, n=7; I3KO, n=5. Statistical significance was evaluated by student's T-test, *p<0.05; **p<0.01; ***p<0.001; ****p<0.0001.

Figure 6. I3IN-002 alters gene expression similar to the genetic knockout.

a. Volcano plots of differentially expressed genes with genetic IGF2BP3 knockout (left) and with I3IN-002 treatment (right) in SEM cells, using DESeq analysis on RNA-sequencing data from SEM cells treated with DMSO, I3IN-002 and SEM/I3KO.

b. Venn diagram of shared differentially expressed genes with IGF2BP3 knockout and I3IN-002 treatment in SEM cells. Hypergeometric test of overlap showed a p-value<10^{-16}.

c. GSEA analysis of the overlapped genes between I3KO and I3IN-002 treated cells.

d-i. RT-qPCR based confirmation of genes showing common differential regulation between I3IN-

002 treatment and genetic knockout of IGF2BP3 (I3KO). Data are shown as fold change, following

normalization to DMSO, with 3 replicate measurements per sample.

j-k. Western blot measurement of differential genes from RNA-seq experiment P4HA1, BTG2, KDM3A, and known IGF2BP3 targets BCL2 and CDK6.

Figure 7. I3IN-002 shows on target activity in biochemical assays.

a. Western blot analysis of RNA immunoprecipitation samples following treatment of SEM cells with 5 μM I3IN-002. Inp represents the input cell lysate; IgG represents a control immunoprecipitation with isotype control: and “IP” represents anti-IGF2BP3 immunoprecipitation.

b. Venn diagram showing significant overlap of differentially expressed genes from I3RIP and I3eCLIP. Hypergeometric test of overlap showed a p-value $<10^{-16}$.

c. Scatter plot of RIP-seq data, plotted as enrichment ratio in DMSO-treated cells (x-axis) versus enrichment ratio in I3IN-002-treated cells (orange dots). Differentially enriched genes with a difference in enrichment ratio of greater than 1 between I3IN-002 and DMSO are shown as green squares. Red triangles indicate genes with an enrichment ratio difference of greater than 1 as well as being identified as IGF2BP3 target mRNAs on prior eCLIP analysis.

d. Quantification of *CDK6* and *BCL2* RNA recovered from RNA immunoprecipitation experiments with or without treatment with I3IN-002.

e. Dual luciferase assay on 3’ UTR of IGF2BP3 targets show decrease in Relative Luciferase activity in the presence of I3IN-002, calculated as Firefly luciferase / Renilla luciferase ratio, and expressed as fold change from DMSO for each UTR. “Vector” represents the empty vector with no 3’UTR, used as a negative control here. Data represents mean and standard error of mean from 6 replicates.

f. Cellular thermal shift assay; Western blots of IGF2BP3 and β-actin are shown following treatment of cells with I3IN-002 or DMSO control, followed by heat-mediated denaturation and removal of denatured protein.

g. Thermal shift assay using purified full-length IGF2BP3 protein.

Figure 1.

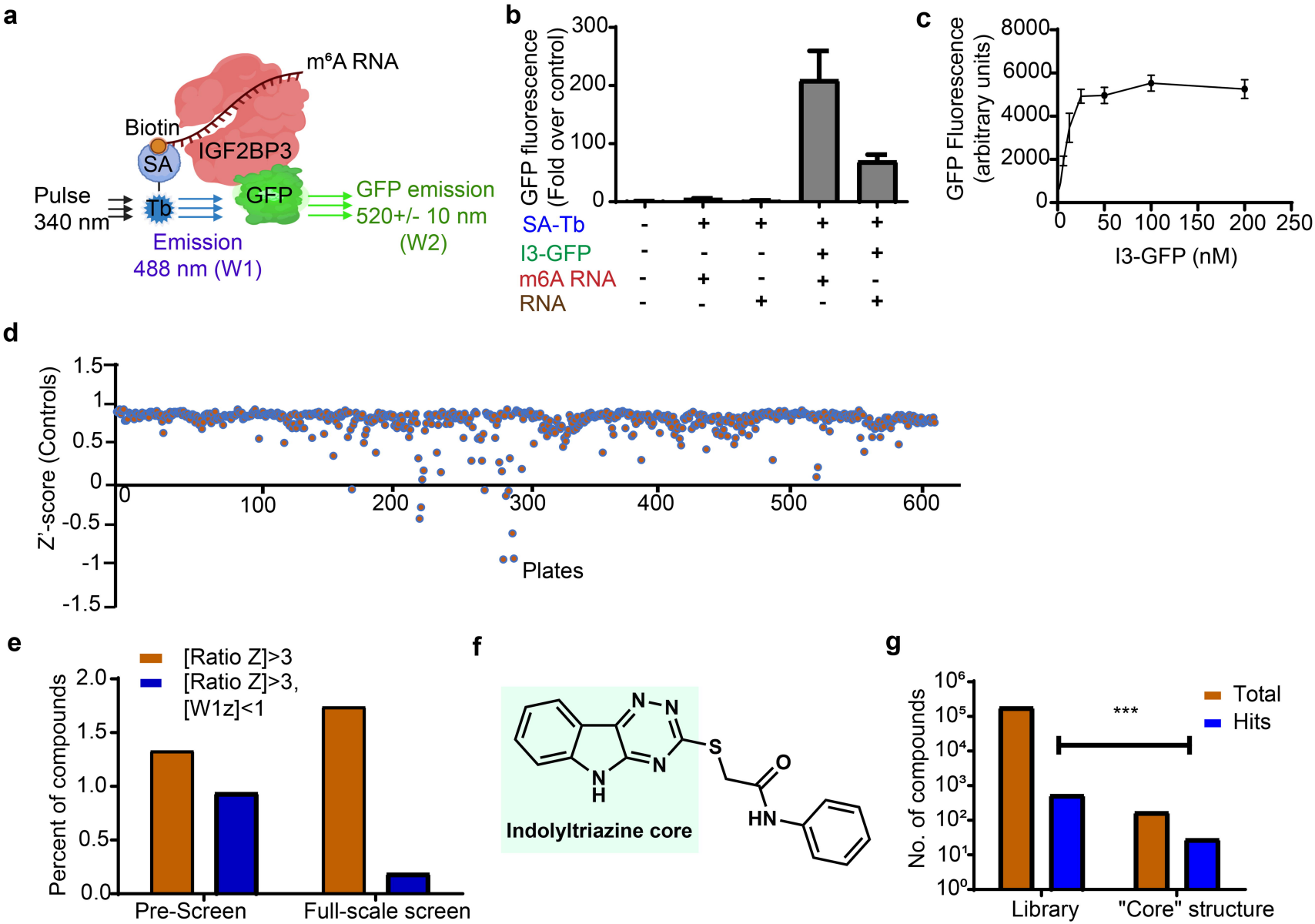
a
m⁶A RNA
Biotin
SA
IGF2BP3
GFP
Pulse
340 nm
Tb
Emission
488 nm (W1)
GFP emission
520+/- 10 nm
(W2)
b
GFP fluorescence
(Fold over control)
300
200
100
0
SA-Tb - + + + +
I3-GFP - - - + +
m6A RNA - + - + -
RNA - - + - +
c
GFP Fluorescence
(arbitrary units)
8000
6000
4000
2000
0
0 50 100 150 200 250
I3-GFP (nM)
d
Z'-score (Controls)
1.5
1
0.5
0
-0.5
-1
-1.5
0 100 200 300 400 500 600
Plates
e
[Ratio Z]>3
[Ratio Z]>3,
[W1z]<1
Percent of compounds
2.0
1.5
1.0
0.5
0.0
Pre-Screen
Full-scale screen
f
N
N
N
H
S
O
HN
Indolyltriazine core
g
No. of compounds
10⁶
10⁵
10⁴
10³
10²
10¹
10⁰
***
Total
Hits
Library
"Core" structure

Figure 2.

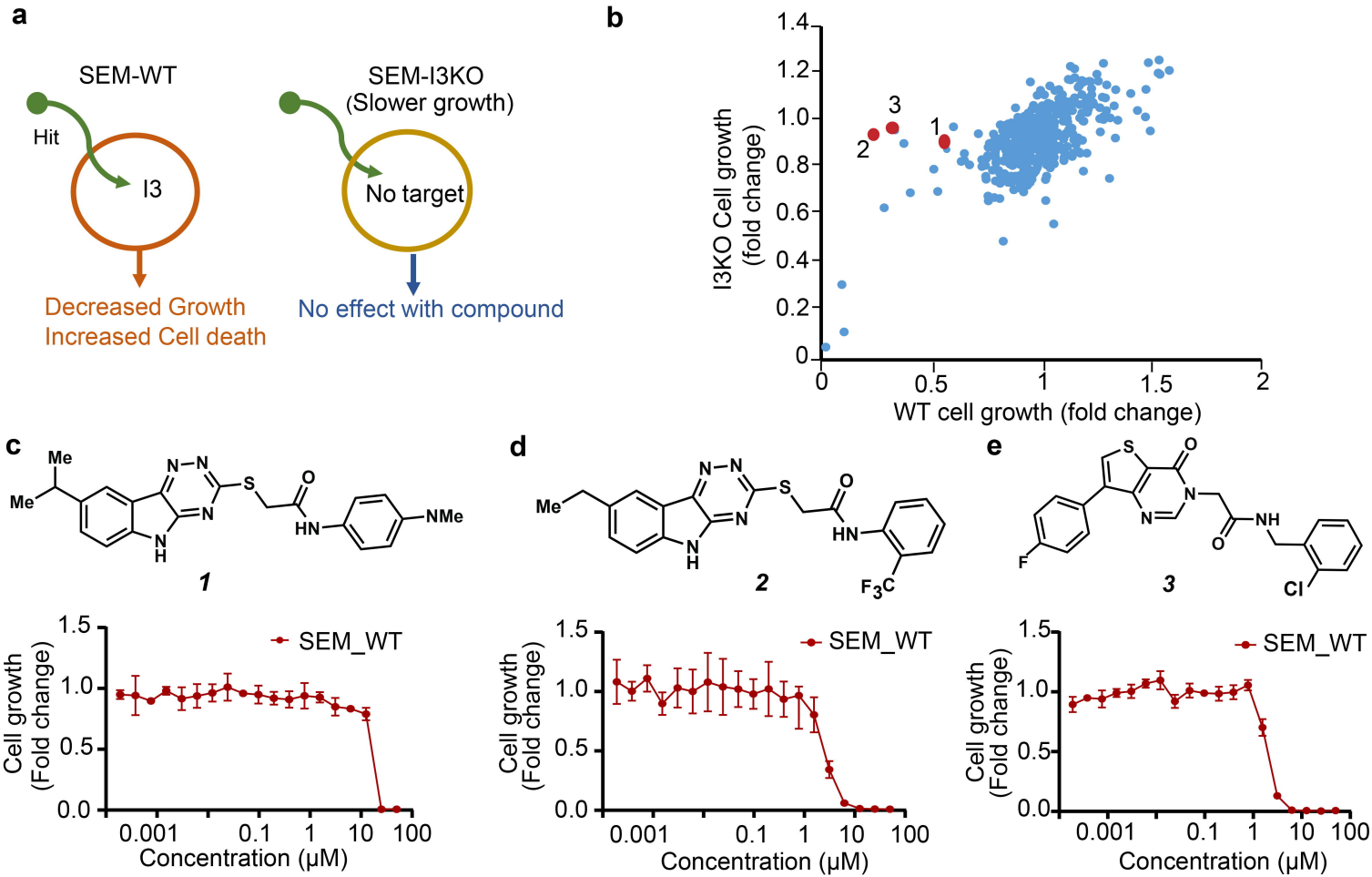
a
SEM-WT
Hit
I3
Decreased Growth
Increased Cell death
SEM-I3KO
(Slower growth)
No target
No effect with compound
b
I3KO Cell growth
(fold change)
WT cell growth (fold change)
1
2
3
c
d
e
1
2
3
SEM_WT
Cell growth
(Fold change)
Concentration (μM)

Figure 3.

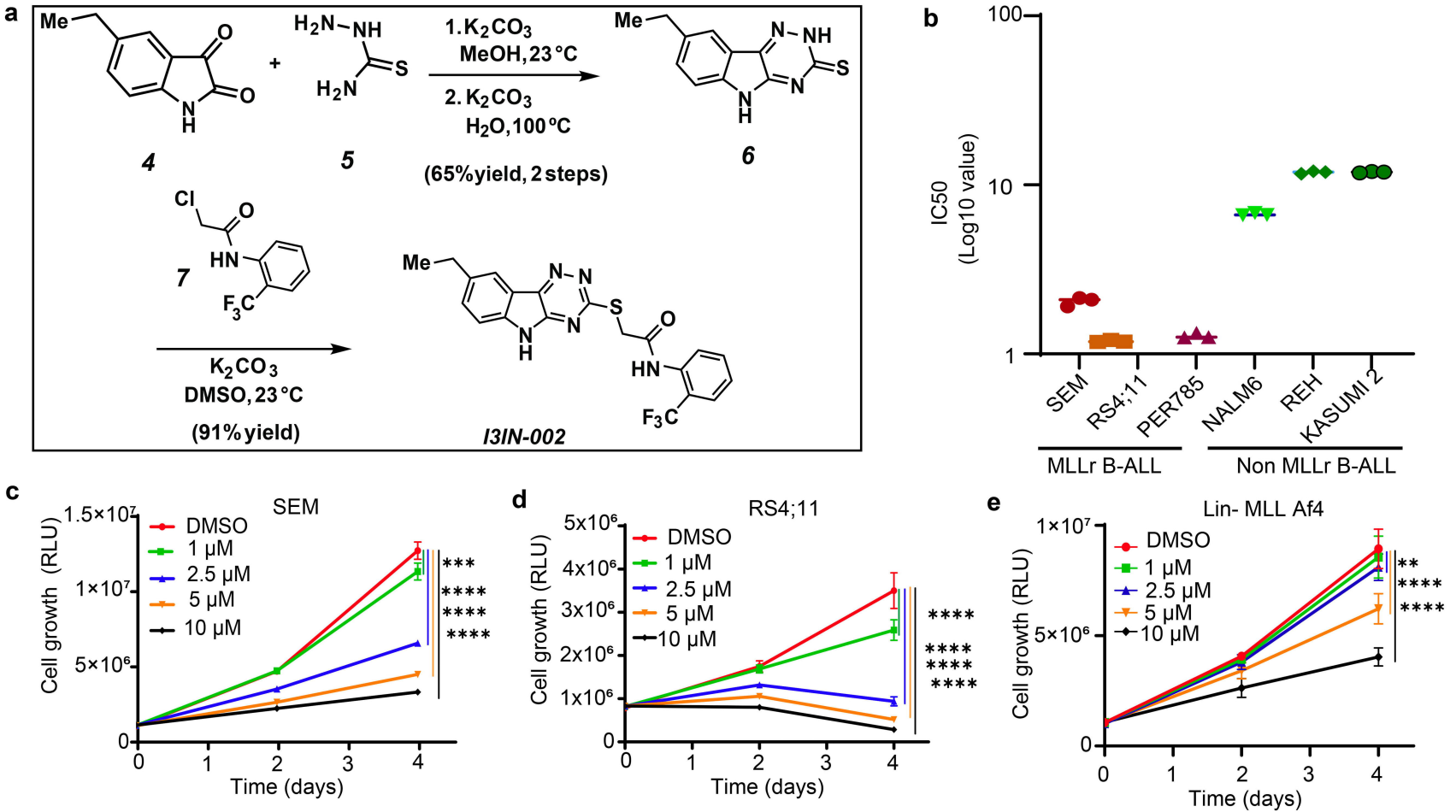
a
Me
O
O
N
H
4
+
H2N–NH
S
H2N
5
1. K2CO3
MeOH, 23 °C
2. K2CO3
H2O, 100 °C
(65% yield, 2 steps)
Me
N–NH
S
N
N
H
6
Cl
O
HN
7
F3C
K2CO3
DMSO, 23 °C
(91% yield)
Me
N–N
S
O
N
N
H
HN
F3C
I3IN-002
b
IC50
(Log10 value)
100
10
1
SEM
RS4;11
PER785
NALM6
REH
KASUMI 2
MLLr B-ALL
Non MLLr B-ALL
c
SEM
Cell growth (RLU)
1.5×10⁷
1×10⁷
5×10⁶
0
DMSO
1 μM
2.5 μM
5 μM
10 μM
***
****
****
****
0
1
2
3
4
Time (days)
d
RS4;11
Cell growth (RLU)
5x10⁶
4x10⁶
3x10⁶
2x10⁶
1x10⁶
0
DMSO
1 μM
2.5 μM
5 μM
10 μM
****
****
****
****
0
1
2
3
4
Time (days)
e
Lin- MLL Af4
Cell growth (RLU)
1×10⁷
5×10⁶
0
DMSO
1 μM
2.5 μM
5 μM
10 μM
**
****
****
0
1
2
3
4
Time (days)

Figure 4

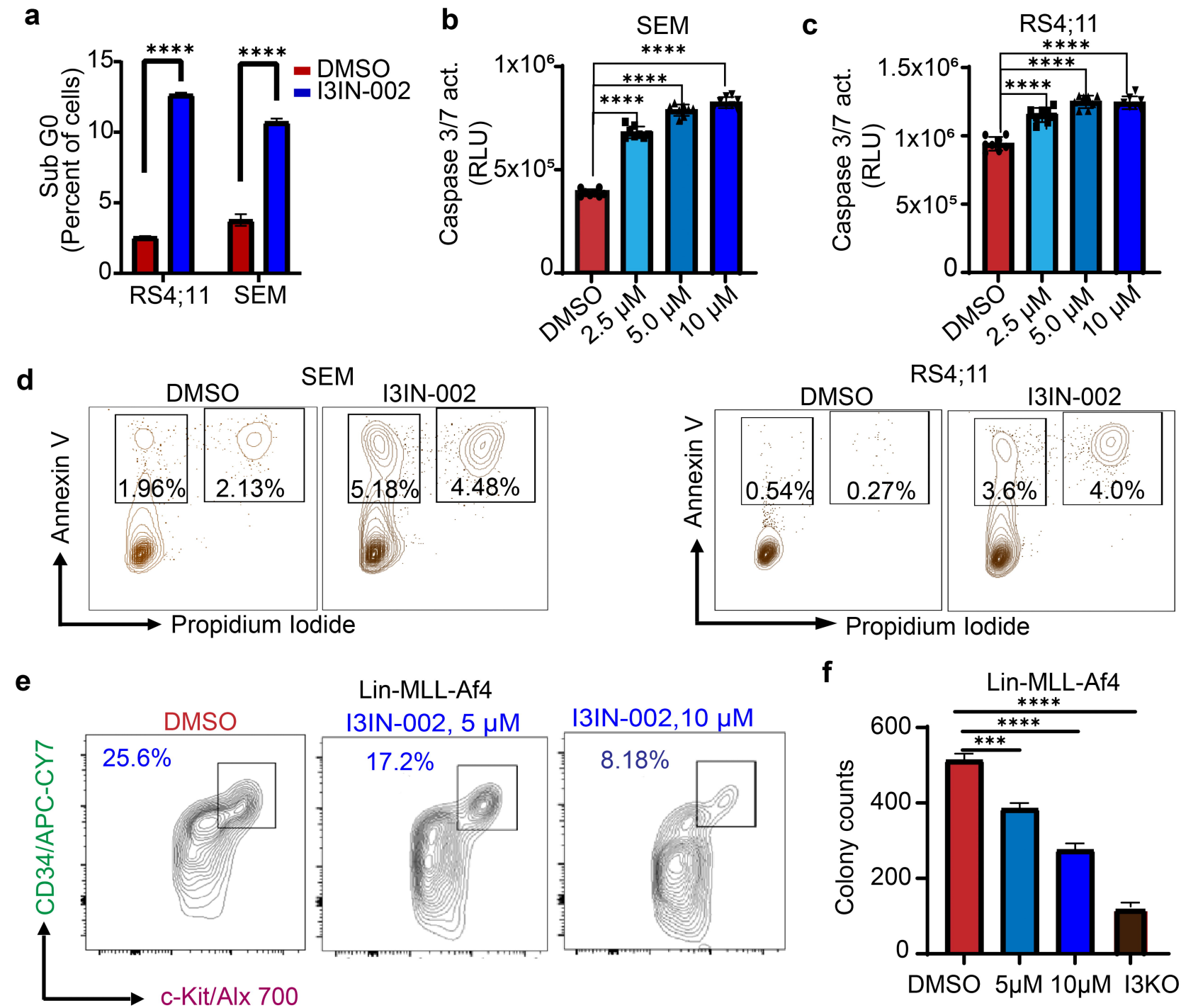
a
Sub G0 (Percent of cells)
15
10
5
0
****
****
DMSO
I3IN-002
RS4;11
SEM
b
SEM
Caspase 3/7 act. (RLU)
1x10⁶
5x10⁵
0
****
****
****
DMSO
2.5 μM
5.0 μM
10 μM
c
RS4;11
Caspase 3/7 act. (RLU)
1.5x10⁶
1x10⁶
5x10⁵
0
****
****
****
DMSO
2.5 μM
5.0 μM
10 μM
d
SEM
DMSO
I3IN-002
Annexin V
1.96%
2.13%
5.18%
4.48%
Propidium Iodide
RS4;11
DMSO
I3IN-002
Annexin V
0.54%
0.27%
3.6%
4.0%
Propidium Iodide
e
Lin-MLL-Af4
DMSO
I3IN-002, 5 μM
I3IN-002,10 μM
25.6%
17.2%
8.18%
CD34/APC-CY7
c-Kit/Alx 700
f
Lin-MLL-Af4
Colony counts
600
400
200
0
****
****
***
DMSO
5μM
10μM
I3KO

Figure 5.

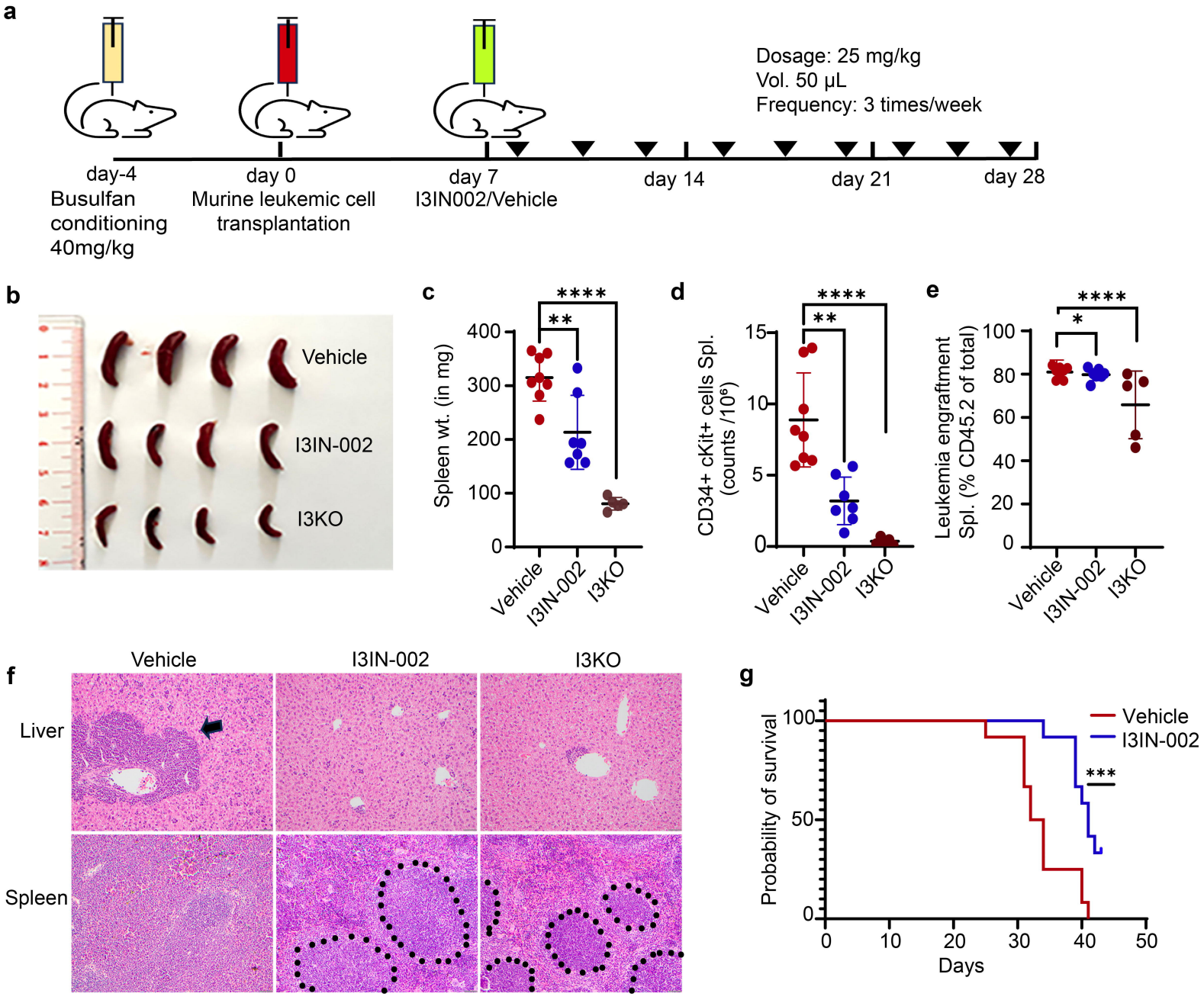
a
Dosage: 25 mg/kg
Vol. 50 µL
Frequency: 3 times/week
day-4
Busulfan conditioning 40mg/kg
day 0
Murine leukemic cell transplantation
day 7
I3IN002/Vehicle
day 14
day 21
day 28
b
Vehicle
I3IN-002
I3KO
c
Spleen wt. (in mg)
d
CD34+ cKit+ cells Spl. (counts /10⁶)
e
Leukemia engraftment Spl. (% CD45.2 of total)
f
Vehicle
I3IN-002
I3KO
Liver
Spleen
g
Probability of survival
Days
Vehicle
I3IN-002

Figure 6.

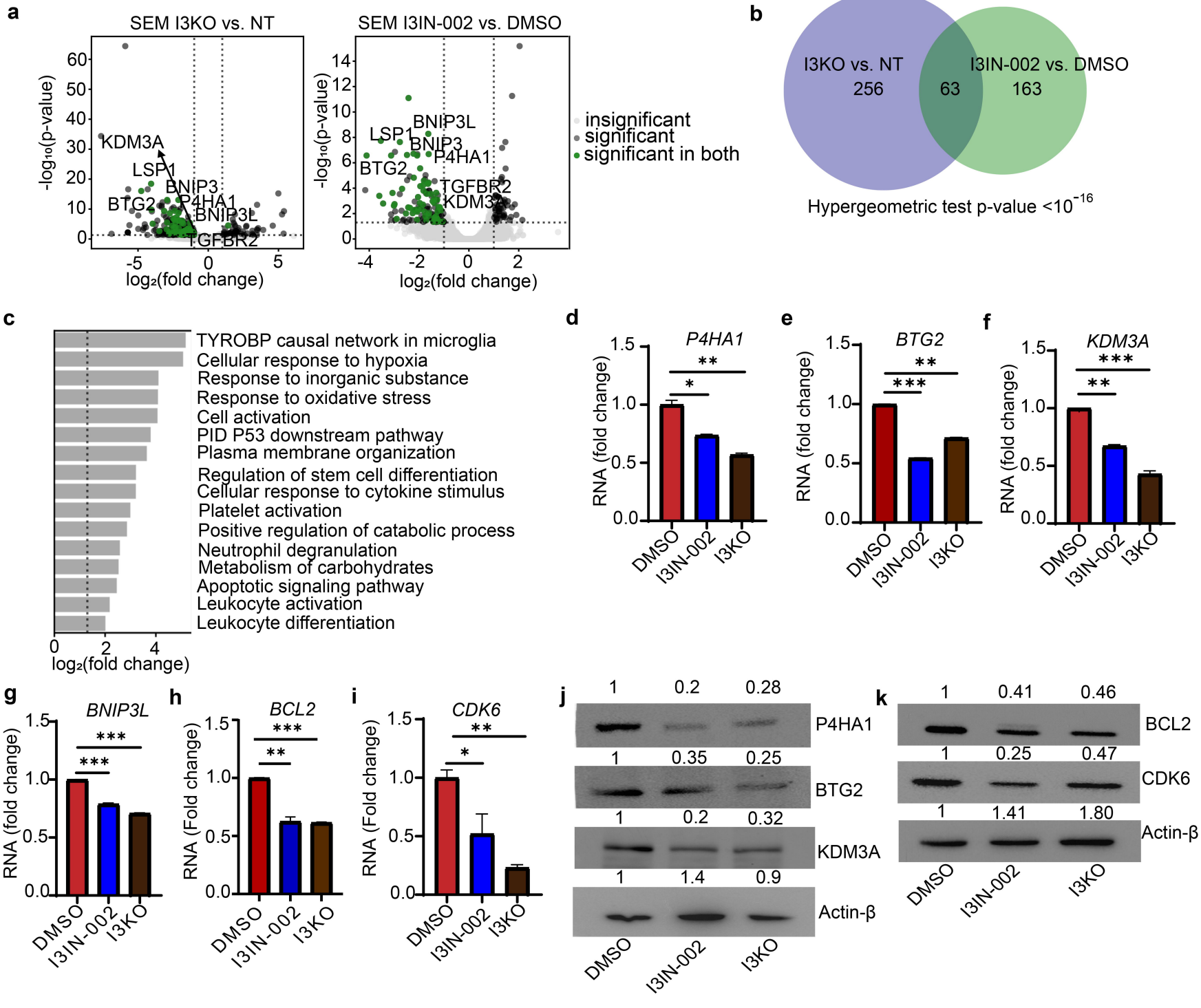
a
SEM I3KO vs. NT
SEM I3IN-002 vs. DMSO
-log10(p-value)
log2(fold change)
KDM3A
LSP1
BNIP3
BTG2
P4HA1
BNIP3L
TGFBR2
insignificant
significant
significant in both
b
I3KO vs. NT
256
63
I3IN-002 vs. DMSO
163
Hypergeometric test p-value <10-16
c
TYROBP causal network in microglia
Cellular response to hypoxia
Response to inorganic substance
Response to oxidative stress
Cell activation
PID P53 downstream pathway
Plasma membrane organization
Regulation of stem cell differentiation
Cellular response to cytokine stimulus
Platelet activation
Positive regulation of catabolic process
Neutrophil degranulation
Metabolism of carbohydrates
Apoptotic signaling pathway
Leukocyte activation
Leukocyte differentiation
log2(fold change)
d
P4HA1
e
BTG2
f
KDM3A
RNA (fold change)
DMSO
I3IN-002
I3KO
g
BNIP3L
h
BCL2
i
CDK6
RNA (Fold change)
j
P4HA1
BTG2
KDM3A
Actin-β
1
0.2
0.28
1
0.35
0.25
1
0.2
0.32
1
1.4
0.9
k
BCL2
CDK6
Actin-β
1
0.41
0.46
1
0.25
0.47
1
1.41
1.80

Figure 7.

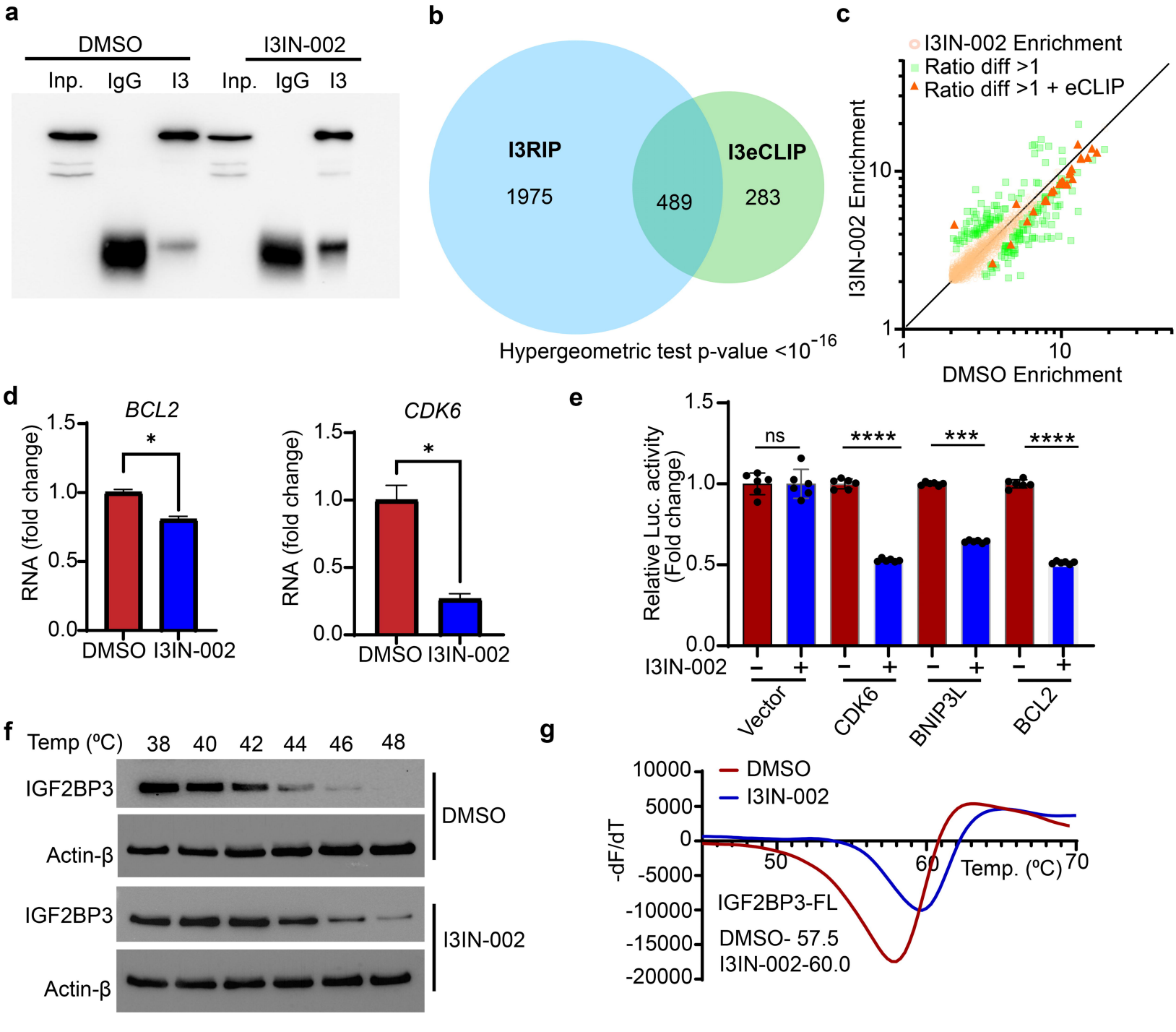
a
DMSO
I3IN-002
Inp.
IgG
I3
Inp.
IgG
I3
b
I3RIP
1975
489
I3eCLIP
283
Hypergeometric test p-value <10-16
c
I3IN-002 Enrichment
Ratio diff >1
Ratio diff >1 + eCLIP
I3IN-002 Enrichment
DMSO Enrichment
1
10
1
10
d
BCL2
CDK6
RNA (fold change)
1.5
1.0
0.5
0.0
*
*
DMSO
I3IN-002
DMSO
I3IN-002
e
Relative Luc. activity (Fold change)
1.5
1.0
0.5
0.0
ns
****
***
****
I3IN-002
–
+
–
+
–
+
–
+
Vector
CDK6
BNIP3L
BCL2
f
Temp (ºC)
38
40
42
44
46
48
IGF2BP3
Actin-β
DMSO
IGF2BP3
Actin-β
I3IN-002
g
DMSO
I3IN-002
10000
5000
0
-5000
-10000
-15000
-20000
-dF/dT
50
60
70
Temp. (ºC)
IGF2BP3-FL
DMSO- 57.5
I3IN-002-60.0

Jaiswal et al., 2025

Supplemental Files Table of Contents

Supplementary Figure 1.

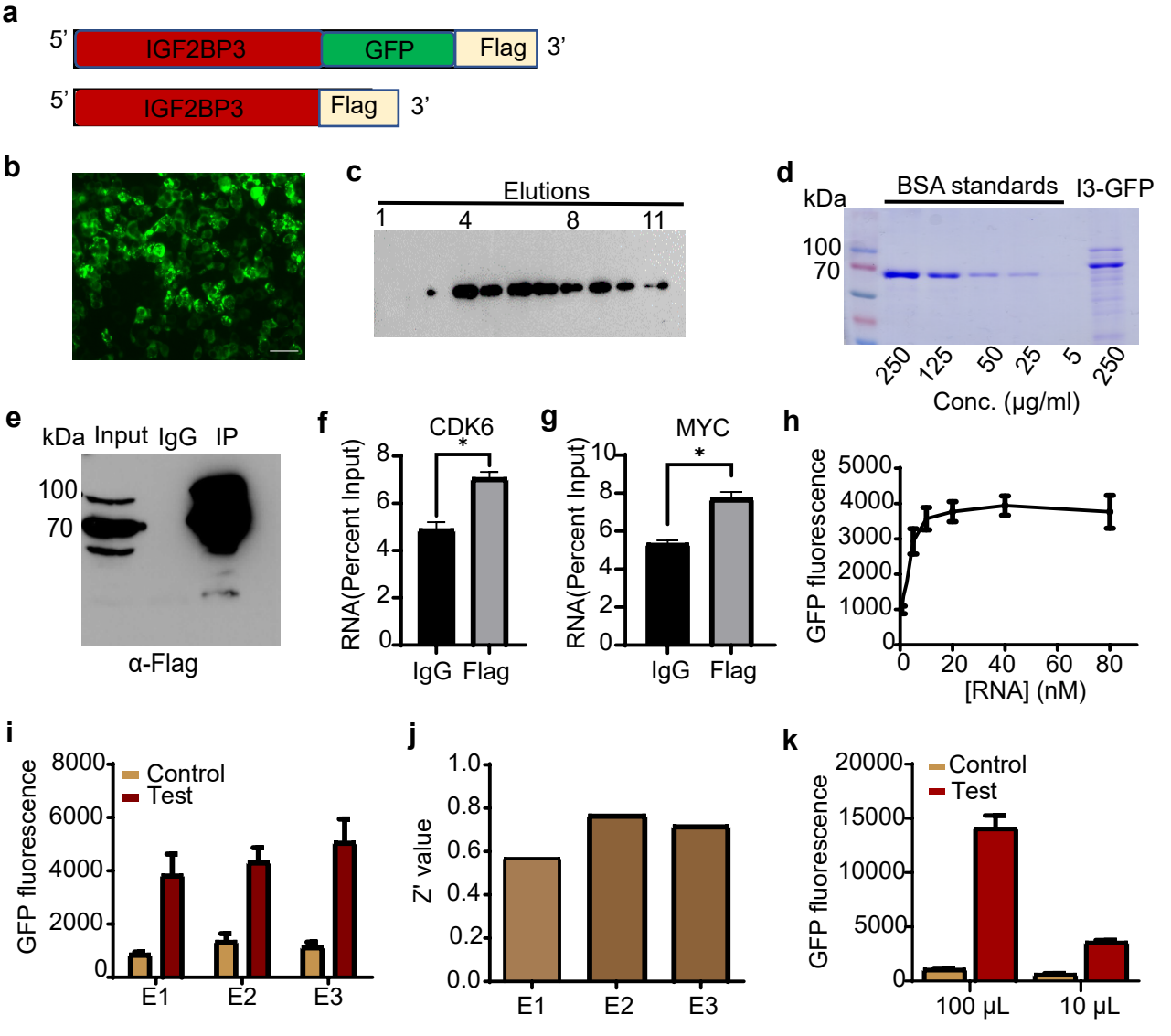

Supplementary Figure 2.

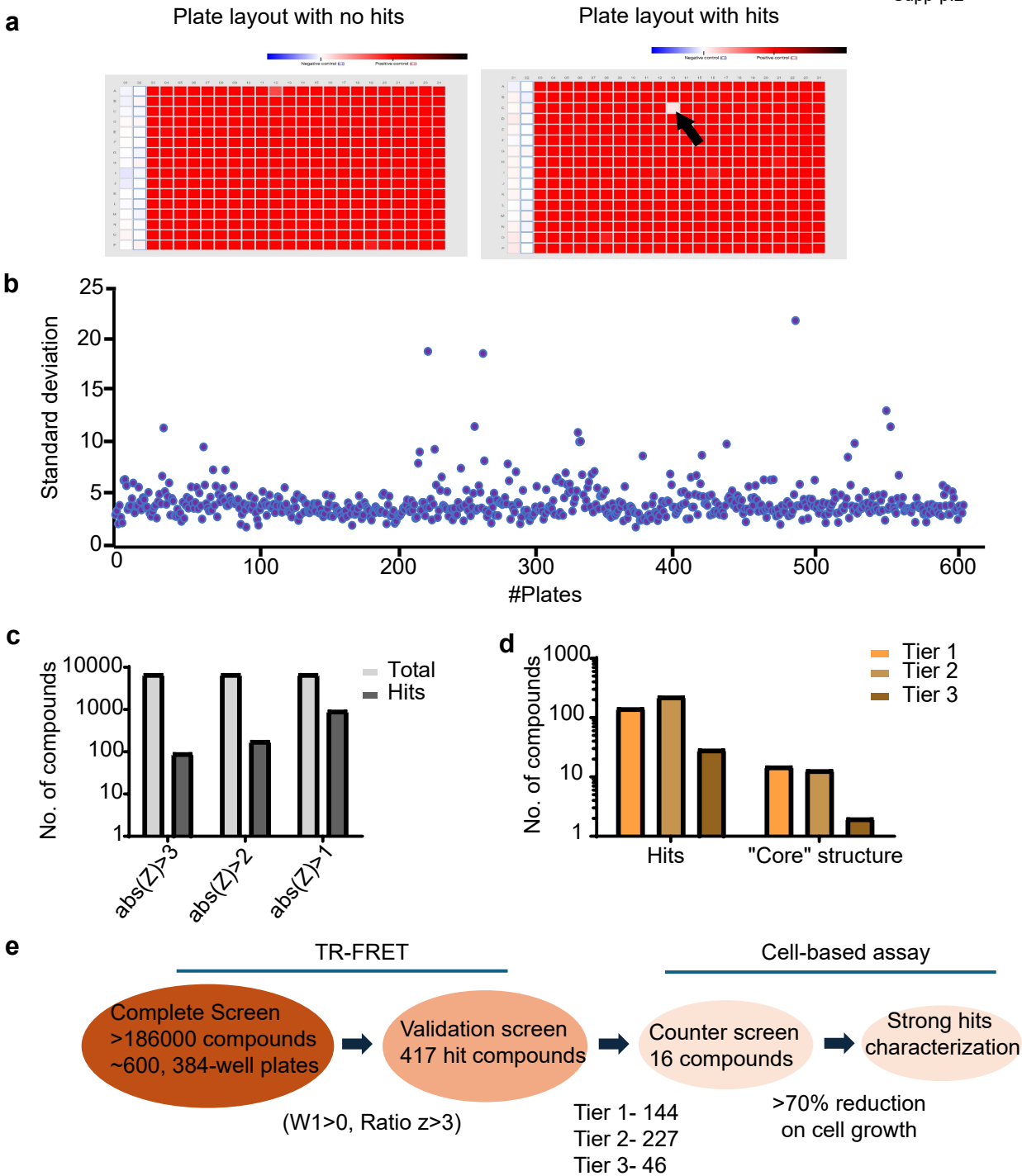

Supplementary Figure 3.

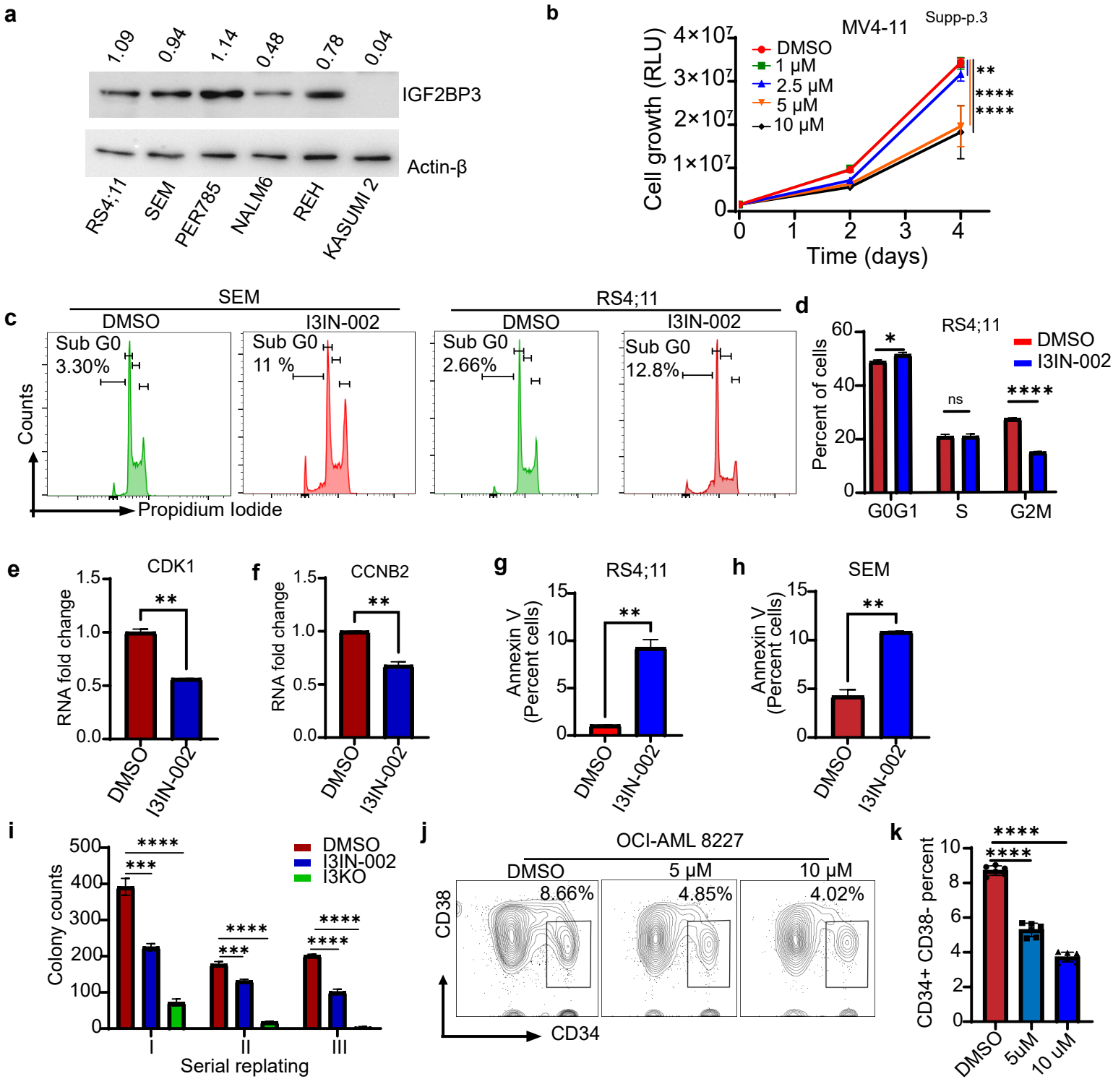

Supplementary Figure 4.

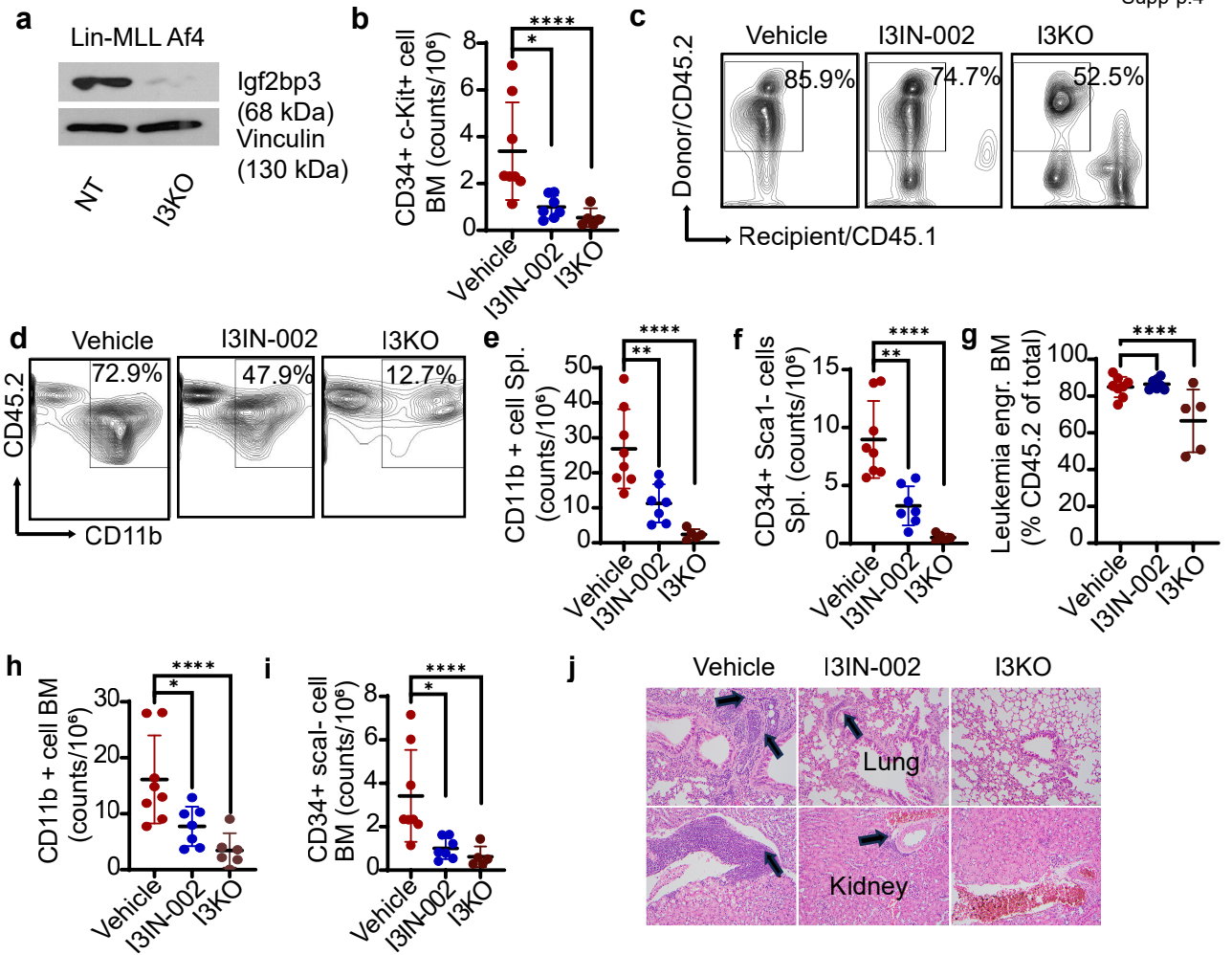

Supplementary Figure 5.

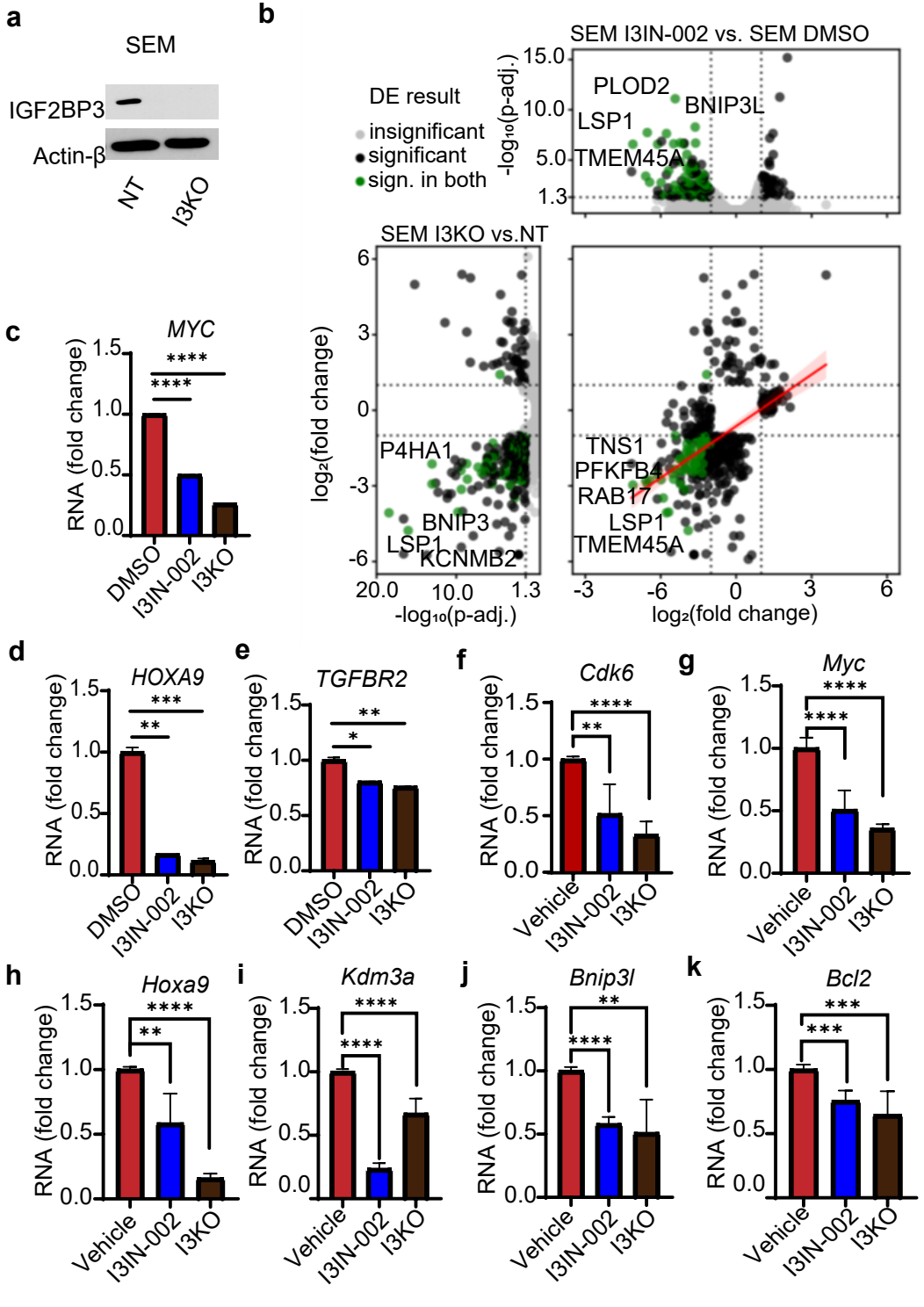

Supplementary Figure 6.

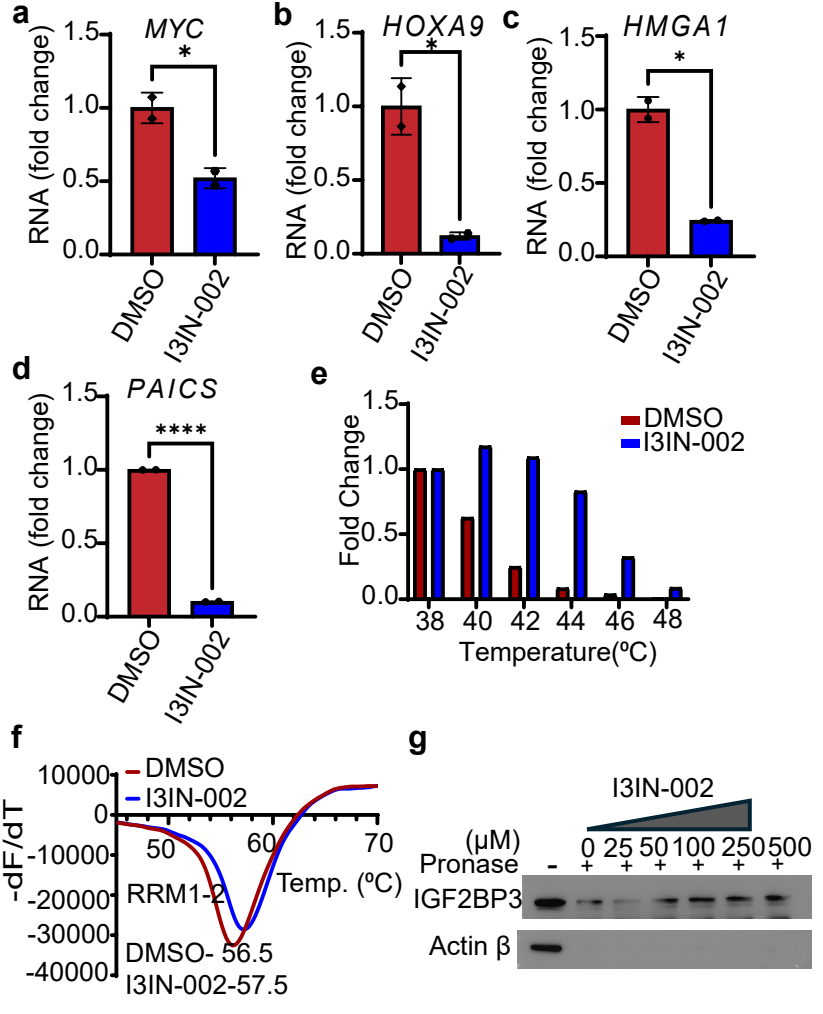

Supplemental Figure Legends.

Supplemental Figure 1, related to Figure 1. Configuration and standardization of TR-FRET assay.

a. Schematic representation of constructs used in protein purification for TR-FRET.

b. Photomicrograph of GFP fluorescence following transfection of plasmid. Scale bar, 50 micron.

c. Western blot analysis for IGF2BP3 in elutions from anti-Flag column.

d. Coomassie stained polyacrylamide gel showing I3-GFP purified from the column.

e-g. RNA immunoprecipitation using purified IGF2BP3 protein (confirmed by Western Blot), (e) of *CDK6* (f) and *MYC* (g) mRNAs, assessed by RT-qPCR.

h. GFP Fluorescence (arbitrary units) as a function of RNA oligonucleotide concentration.

i-j. GFP fluorescence and Z' values in three different experiments performed on three different days (E1-E3; n=110 (replicates); assay volume= 10 µL)

k. Comparison of GFP fluorescence in 100 µL and 10 µL assay volume**.**

Supplemental Figure 2. High throughput screening assay, related to Figure 1.

a. Plate layout and example plate with hit (right). Please see materials and methods for further details.

b. Plot of plate standard deviations across 600+ plates used for the assay.

c. Number of compounds identified as hits by different cut-off criteria in preliminary screening experiment. Based on established literature and these results a cut-off of $|z|>3$ was chosen.

d. To confirm hits identified in the full-scale screen, several replicate experiments were carried out to assess changes in fluorescence ratios. 417 high-probability hits were re-pinned into two 384-well plates and were subjected to the same TR-FRET assay as before. An individual compound was defined as being a "hit" in the validation screen when the fluorescence ratio deviated from negative controls by greater than three standard deviations. Next, we defined a

Tier 1 hit compound as positive in both experimental replicates; Tier 2 hit compound as positive in 1 out of 2 experimental replicates, and Tier 3 compounds were “non-hits” in the validation experiment based on their not being positive in either replicate. The relative frequency of Tier 1, Tier 2 and Tier 3 compounds amongst all “primary hits” versus amongst compounds with “Core structure” are plotted here.

e. Overall strategy of TR-FRET screen, validation, and counter-screen.

Supplemental Figure 3. Characterization of anti-leukemic effects of I3IN-002, related to Figure 3 and Figure 4.

a. Baseline expression of IGF2BP3 in B-ALL and AML cells.

b. Concentration dependent alterations of cell growth curves over 4 days of cell culture with I3IN-002 treatment, assessed by CellTiterGlo assay, and plotted as relative luminescence units (RLU) in MV4-11.

c. FACS-based cell cycle analysis following treatment with I3IN-002 versus control, with histograms of propidium iodide staining in SEM and RS4;11 cells.

d. Quantification of percentage of RS4;11 cells at each stage of cell cycle with 3 replicates.

e-f. G2-M transition genes CDK1 and CCNB2 downregulated in I3IN-002 treatment.

g-h. Quantitation of total Annexin V positivity in RS4;11 and SEM cells following treatment with I3IN-002. Data represents mean and standard error of mean with 3 replicates.

i. Decreased colony counts upon serial replating in different treatment groups

j-k. FACS histogram and quantitation, respectively, of a leukemic stem-cell enriched population by assaying the CD34+ CD38- population following in vitro treatment of OCI-AML-8227 cells in culture.

Supplemental Figure 4. Further characterization of in vivo phenotypes related to Figure 5.

a. Western blot showing Igf2bp3 expression in NT and Igf2bp3 knockout Lin- MLL- Af4 cells.

b. Absolute counts of CD34+ cKit+ leukemic cell in bone marrow compartment.

c. FACS histograms of CD45.1/CD45.2 congenic marker staining for measurement of leukemia engraftment.

d. FACS histograms of CD45.2/CD11b staining for measurement of leukemia engraftment.

e-f. Absolute counts of CD11b and CD34+ Sca1- cells in spleen compartments.

g. Percent quantification of Leukemic engraftment in the bone marrow.

h-i. Absolute counts of CD11b and CD34+ Sca1- cells in bone marrow compartments.

j. Histologic sections of lung and kidney comparing the morphology of tissues following engraftment of leukemia and treatment with vehicle, I3IN-002, or genetic deletion of IGF2BP3. Arrows show areas of leukemic infiltration. Hematoxylin and eosin staining, original magnification, 200X.

Supplemental Figure 5. Characterization of on-target activity of IGF2BP3, related to Figure 6.

a. IGF2BP3 expression in NT and IGF2BP3 KO SEM cells.

b. Volcano plots of differentially expressed genes with genetic IGF2BP3 knockout (left) and with I3IN-002 treatment (top) in SEM cells, using DESeq analysis on RNA-sequencing data from SEM cells treated with DMSO, I3IN-002 and SEM/I3KO.

c-d. RT-qPCR analysis for *MYC* and *HOXA9* from RNA immunoprecipitation sample..

e. RT-qPCR of additional genes *TGFBR2* identified from differential expression analyses of RNA-sequencing experiments.

f-k. RT-qPCR analyses of RNA isolated from mouse spleen following in vivo treatment described in **Fig. 5**. Three representative mice from each group were selected for the RT-qPCR analyses.

Supplemental Figure 6. **Characterization of on-target activity of IGF2BP3, related to Figure 6.**

a-d. RT-qPCR analysis for *MYC*, *HOXA9, HMGA1 and PAICS* from RNA immunoprecipitation sample.

e. Quantification of Western blot bands from Cellular thermal shift assay.

f. Thermal shift assay on purified RRM 1-2 domain of IGF2BP3.

g. Drug affinity responsive target stability show I3IN-002 protects IGF2BP3 from Pronase activity.

Detailed description of Methods

Cell lines and cell culture

All cell lines were maintained in standard conditions in incubator at 37 °C and 5% CO_2. Human B-ALL cell lines, RS4;11 (ATCC CRL-1873), NALM6 (ATCC CRL-3273), SEM (DMZ-ACC 546), PER785 , REH (ATCC CRL-8286), MV4;11 (ATCC CRL-9591), and KASUMI 2 (DSMZ ACC 526) were cultured as previously described (1-4). Immortalized MLL-Af4 transformed hematopoietic stem and progenitor cells derived from mouse bone marrow (MLL-Af4 Lin- cells) were cultured in IMDM with 15% FBS, supplemented with recombinant mouse stem cell factor (SCF, 100 ng/mL, Thermo Fisher), recombinant mouse Interleukin-6 (IL-6, 4 ng/mL, Thermo Fisher), recombinant human FMS like tyrosine kinase 3 ligand (FLT3-L, 50 ng/mL, Thermo Fisher) and mouse thrombopoietin (TPO,50 ng/mL, Thermo Fisher). OCI-AML8227 cells were a kind gift from Dr. John Dick and Dr. Eric Lechman (5). OCI-AML 8227 cells were cultured in a specialized media AMEM (Wisent Bio), BITS 9000 (Stem Cell Technologies), stem cell factor (SCF, 200 ng/mL, R&D systems), thrombopoietin (TPO, 25 ng/mL, R&D systems), FMS like tyrosine kinase 3 ligand (FLT3-L, 50 ng/mL, R&D systems), Interleukin-6 (IL-6, 20ng/mL, R&D systems), interleukin-3 (IL-3, 10 ng/mL, R&D systems), granulocyte Colony- Stimulating Factor (G-CSF, 10 ng/mL, R&D systems). OCI-AML8227 cells were cultured by plating 450000 cells/well of non-tissue culture treated 24-well plate (Eppendorf co.) and were passaged every 7 days. These are further listed in **Supp. Table 1**.

CRISPR/Cas9-mediated deletion of IGF2BP3 in cell lines

Human B-ALL cell lines SEM, RS4;11, and NALM6 were depleted for IGF2BP3 using lentiviral delivery of CRISPR/Cas9 components in a two-vector system and sgRNA sequence as previously described (1, 6). Immortalized MLL-Af4 Lin- cells were initially isolated from bone marrow of Cas9-GFP mice and then transformed using retroviral transduction with MLL-Af4 retroviral supernatant, with four rounds of transduction with MLL-Af4 retroviral supernatant, followed by selection in G418

supplemented media at 400 µg/mL for 7 days, as previously described. Cells were then stably transduced with lentiviral supernatant containing sgRNA against *Igf2bp3* (I3Cr2) or non-targeting (NT-1), and sorted on GFP and mCherry positivity (1, 6).

Protein over-expression and purification

IGF2BP3-GFP-Flag over-expression plasmid was constructed by fusing full length IGF2BP3 CDS with GFP CDS and cloned in pCDNA 3.0 vector. pCDNA3/IGF2BP3.GFP.Flag construct was transfected in 293T cells plated in 150 mm tissue culture dish. After 48 hours of transfection, cells were lysed in non-denaturing lysis buffer (50 mM Tris- HCl, pH 7.4, 300 mM NaCl, 5% glycerol, 0.1% NP40, 1X DNase, 10 units RNase/mL, 7.0 mg/50 mL of DTT, 1x Protease inhibitor) and incubated on ice for 1 hour. followed by 25 cycles of sonication with 10 seconds. 'on' and 20 seconds. 'off' pulse. Lysate was cleared by centrifugation at 12,000 x g for 15 minutes. Cleared lysates were loaded in the column filled with Anti-FLAG M2 resin (Sigma Aldrich) and passed multiple times to assist the binding. The bound protein fraction was eluted by adding 0.5 M Glycine HCl, pH 3.5 buffer. The eluent was concentrated using Vivaspin MwCO 50 column (Greiner Bio One). The concentrated protein was stored in 100 mM Tris-HCl buffer at pH 7.2. The purity and integrity of the protein was determined by mass spectroscopy and SDS-PAGE Commassie staining. The specificity of the purified protein was determined by western blotting and probing for IGF2BP3 using rabbit Anti-human IGF2BP3 antibody.

Protein extraction and Western blot

Cell lysates were made in non-denaturing cell lysis buffer and RIPA lysis buffer. Lysates were electrophoresed using SDS-PAGE using standard conditions (7). A comprehensive list of antibodies is provided in **Supp. Table 2**.

TR-FRET assay

TR-FRET assay was performed using the purified IGF2BP3-GFP fusion protein**.** Briefly, FRET assay was performed in assay buffer (50mM Tris-HCl, pH 7.4, 150 mM NaCl, DTT, 5% Glycerol, protease inhibitor (1x), RNase Inhibitor (10u/mL)). First, the purified protein was diluted at 50 nM concentration (2x) in the assay buffer and added to the plate. In the second step, 20 nM (2x) concentration of biotinylated M6A labelled RNA oligo (**Supp. Table 3**) was incubated with Streptavidin-Terbium in the assay buffer for 30 mins. on ice. After the incubation was over, the Streptavidin-Tb + RNA complex was added to the wells with purified proteins. The plate was incubated for 1 hr. at RT for binding and read on EnVision microplate reader (Perkin Elmer) with a dual PMT configuration using a 340 nm excitation and a dual emission mirror block with using a 495 nm emission filter for Terbium fluorescence (W1 channel) and a 525 nm emission filter for GFP fluorescence (W2 channel). The measurement details were as follows: 2000 cycles, 120 flashes, 200 us delay and 300 us total time window. Excitation and emission light were set to 100%. The assay was miniaturized to 10uL in 384-well plates and an in-house compound deck at UCLA MSSR was applied to the assay, with parameters as described in Results.

Data analysis of HTS assays

Values for W2, W1 and the ratio of W2 to W1 for each compound, DMSO and no IGF2BP3-GFP controls were imported into our Collaborative Drug Discovery platform for each plate and Z' for each plate determined. Z'<0.5 were flagged for repeats. Plates were normalized for Teribum (W1), GFP (W2) and W2/W1 ratios (Ratio), prospective hits were flagged for further analysis with a |Ratio Z| > 3 (Primary criterion). The secondary criterion was |W1 Z|<1 (where the mean and standard deviation were calculated for either each plate or for all the plates run on a given experiment). The "alternative secondary criterion" used the mean and standard deviation for all plates in a given experiment. Compounds with very strong inhibition in the W1 channel were treated as likely TRF-donor quenchers and de-prioritized. Compounds with very bright W2 signal were similarly treated as non-specifically fluorescent compounds. The residual structures of

prospective hit compounds were exported for review by medicinal chemists and analysis through structure activity landscape index (SALI) plots(8). Following the identification of hits based on these parameters, we then designed a custom set of plates with compounds picked from the in house deck. The confirmatory TR-FRET screens were performed in triplicate with further analysis as described in the results section.

Counter-Screen and Cell-based Assays.

A custom set of plates was constructed from the hits that were identified from the initial TR-FRET based assays. Wild type and IGF2BP3-deleted SEM cell lines (6) were treated with compound, grown for 4 days under normal growth conditions, and assayed for cell growth in 384-well plates with CellTiter-Glo, a luminescence-based reagent described previously (1, 6, 9). Fold change from control (i.e., no compound treated wells) was plotted for SEM-WT versus SEM-I3KO. We utilized the cutoffs described in the results section to enable downstream analysis of potential lead compounds.

Synthesis of I3IN-002

Commercially available reagents were used as received. Methanol (MeOH) was purchased from Fischer Scientific. Deionized water was used. Dimethyl sulfoxide (DMSO) was purchased from Sigma-Aldrich. K_2CO_3 was purchased from Oakwood Chemical. 5-Methyl isatin **4** and α-chloro amide **7** were purchased from Combi-Blocks. Thiosemicarbazide (**5**) was purchased from AK Scientific. Reaction temperatures above 23 °C were controlled using an IKAmag temperature modulator, and unless stated otherwise, performed at room temperature (approximately 23 °C). ^{1}H-NMR spectra were recorded on Bruker spectrometers (at 500 MHz) and are reported relative to the residual solvent signal. Data for ^{1}H-NMR spectra are reported as follows: chemical shift (d ppm), multiplicity, coupling constant (Hz), and integration. ^{13}C-NMR spectra were recorded on Bruker spectrometers (at 125 MHz) and are reported relative to the residual solvent signal. Data

for ^{13}C-NMR spectra are reported as follows: chemical shift (d ppm) and, when necessary, multiplicity and coupling constant (Hz). ^{19}F-NMR spectra were recorded on Bruker spectrometers (at 564 MHz) and are reported relative to the residual solvent signal. Data for ^{19}F-NMR spectra are reported as follows: chemical shift (d ppm) multiplicity and integration. IR spectra were recorded on a Perkin-Elmer UATR Two FT-IR spectrometer and are reported in terms of frequency absorption (cm^{-1}). DART-MS spectra were collected on a Thermo Exactive Plus MSD (Thermo Scientific) equipped with an ID-CUBE ion source and a Vapur Interface (IonSense Inc.). Both the source and MSD were controlled by Excalibur software version 3.0. The analyte was spotted onto OpenSpot sampling cards (IonSense Inc.) using CH_2Cl_2 as the solvent. Ionization was accomplished using UHP He plasma with no additional ionization agents. The mass calibration was carried out using Pierce LTQ Velos ESI (+) and (–) Ion calibration solutions (Thermo Fisher Scientific). Retention times for liquid chromatography were recorded with a Shimadzu Nexera XR equipped with a PDA detector. Chromatography was conducted using a 0.5 mL/min flow rate at 40 °C and Shimadzu Nexcol C18 (1.8 x 50 mm, 2.1 µm) column. Two mobile phase solutions were used: solution A 0.1% formic acid in water and solution B was 0.1% formic acid in acetonitrile. The elution program consisted of a linear gradient starting at 95% A 0.5 min following injection to 5% A over 4 min. All the final compounds presented a purity of at least 95%, determined by HPLC and ^{1}H NMR. Uncorrected melting points were measured using a Digimelt MPA160 melting point apparatus.

A round-bottom flask containing a magnetic stir bar was charged with K_2CO_3 (1.52 g, 11.0 mmol, 1.1 equiv), isatin **4** (1.75 g, 10.0 mmol, 1.0 equiv), thiosemicarbazide **5** (911 mg, 10.0 mmol, 1.0 equiv,) and MeOH (17 mL, 0.60 M). The reaction mixture was allowed to stir at 23 °C for 18 h. At this point, the reaction mixture was acidified by dropwise addition of acetic acid over roughly 5 min (5 mL). The resulting mixture was stirred for 1 hour. After 1 h, the mixture was vacuum filtered over a fritted funnel, and the filter cake containing the product was washed with H_2O (100 mL), followed by Et_2O (50 mL) to afford (E)-2-(5-ethyl-2-oxoindolin-3-ylidene) hydrazine-1-

carbothioamide (2.10 g, crude mass) as a yellow-orange solid. This was used directly in the subsequent reaction without further purification.

To a round-bottom flask containing a magnetic stir bar, (E)-2-(5-ethyl-2-oxoindolin-3-ylidene) hydrazine-1-carbothioamide (2.10 g, 8.46 mmol, 1.0 equiv.) and K_2CO_3 (1.17 g, 8.46 mmol, 1.0 equiv) were added, and dissolved in H_2O (100 mL, 0.08 M). The reaction vessel was fitted with a reflux condenser and the reaction mixture was stirred at 100 °C for 16 h. At this point, the crude mixture was allowed to cool to 23 °C. It was acidified by the dropwise addition of acetic acid over roughly 5 min (10 mL) and then stirred for an additional hour. The mixture was vacuum filtered over a fritted funnel, and the filter cake containing the product was washed with H_2O (100 mL), followed by Et_2O (50 mL) to afford triazinoindolothione **6** (1.47 g, 65% yield over two steps, >95% purity) as a yellow-orange solid.

To a 1-dram vial charged with a magnetic stir bar was added triazinoindolothione **6** (50 mg, 0.22 mmol, 1.0 equiv), α-chloroacetamide **7**(52 mg, 0.22 mmol, 1.0 equiv), K_2CO_3 (60 mg, 0.43 mmol, 2.0 equiv), and DMSO (1.1 mL, 0.20 molar). The reaction mixture was allowed to stir at 23 °C for 16 h. The reaction mixture was transferred to a vial containing H_2O (5 mL), which led to the formation of a precipitate. The mixture was sonicated for 5 minutes to afford the crude product as a suspension in water. This mixture was then heated to reflux for ~ 5 seconds to effect partial dissolution, and was then allowed to cool to 23 °C under ambient conditions. The product precipitated and was collected by vacuum filtration over a paper filter. The filter cake was successively washed with H_2O (5 x 1 mL), MeOH (1 x 0.5 mL), and Et_2O (2 x 1 mL) to give **I3IN-002** (42 mg, 45% yield, >95% purity) as a tan solid. **I3IN-002**: Mp: 253 °C; ^{1}H NMR (500 MHz, $(CD_3)_2SO$): δ 12.54 (s, 1H), 9.90 (s, 1H), 8.14 (s, 1H), 7.72 (d, *J* = 7.8 Hz, 1H), 7.68 (t, *J* = 7.8 Hz, 1H), 7.60 (d, *J* = 8.0 Hz, 1H), 7.56 (dd, *J* = 8.3, 1.4 Hz, 1H), 7.51 (d, *J* = 8.3 Hz, 1H), 7.44 (t, *J* = 7.6 Hz, 1H), 4.27 (s, 2H), 2.80 (q, *J* = 7.5 Hz, 2H), 1.27 (t, *J* = 7.6 Hz, 3H); ^{13}C NMR (125 MHz, $(CD_3)_2SO$): δ 167.3, 165.9, 146.6, 141.3, 138.7, 138.4, 135.2, 133.1, 131.2, 129.3, 126.6, 126.3

(q, *J* = 5.0 Hz), 124.0 (q, *J* = 29.6 Hz), 123.5 (q, *J* = 273.4 Hz), 120.1, 117.6, 112.6, 34.5, 28.0, 16.2; ^{19}F NMR (564 MHz, $(CD_3)_2SO$): δ –59.4 (s, 3H); IR (Film): 3263, 2961, 1662, 1536, 1095 cm^{-1}; HRMS-APCI (*m/z)* $[M + H]^+$ calcd for $C_{20}H_{17}F_3N_5OS^+$, 432.11004; found 432.11002; HPLC purity 97 %; R_t = 4.20 min.

In vitro assays for cell viability, cell cycle apoptosis, and proliferation, with small molecule treatment

Cell viability assays were performed using a luminescent assay based on ATP quantitation (CellTiterGlo, Promega, catalog G7571), per manufacturer's protocol. 1500 cells/well (for 384 well format) and 5000 cells/well (for 96 well format) were plated and incubated with different concentrations of small molecule for four days at 37°C in a 5% CO_2 incubator, followed by endpoint assay. For IC_{50} determinations, small molecule was added at concentrations from 50 μM-0.0004 μM, with 2-fold dilutions. For cell cycle analysis, SEM and RS4;11 cells were treated with 5 μM concentration of I3IN-002 and DMSO for 48 hrs. After 48 hrs. cells were harvested, washed with PBS, and fixed in pre-chilled 70% ethanol overnight. Fixed cells were washed with PBS and 350 μL Propidium Iodide staining solution (20 μg/mL of propidium Iodide and 200 μg/mL of DNase free RNase) was added to the cells and incubated for 1 hr. at RT. Stained cells were run on the flow cytometer and analyzed using FlowJo software V10.

Apoptosis

Apoptosis assays were performed using luminescence-based Caspase Glo assay (Promega). Briefly, SEM and RS4;11 cells were treated with 5 μM concentration of I3IN-002 and DMSO for 48 hrs. Post treatment, 100 μL of Caspase Glo reagent was added to each well (1:1) and incubated for 1 hr. at 37 degree Celsius. Plate was read on Varioscan lux microplate reader from Thermo Scientific. The increase in luminescence in I3IN-002 treated cells compared to DMSO

corresponds to an increase in Caspase 3/7 activity. An alternate measurement of apoptosis was performed on the compound treated cells using Annexin V and propidium iodide staining as described previously(1).

Colony formation assay

Colony formation assay with serial replating was performed using murine Lin-MLL-Af4 cells(6). Briefly, 6000 cells were resuspended in 4 mL of Methocult media (M3434, Stem Cell Technologies) with DMSO/I3IN-002. Then, 1.1 mL of the cell suspension was plated in each 35 mm petri dish and incubated for 8 days. After colony counting, colonies were pooled by adding PBS at room temperature, creating a single-cell suspension by gently mixing with a micropipette, and centrifuging at 1200 rpm for 5 minutes. The pellet was resuspended in PBS, and viable cells were counted using Trypan blue. For serial replating, 1600 cells were seeded again following the previously mentioned steps with DMSO and I3IN-002 (10).

Animal Experiments

For in vivo studies, C57BL/6J, B6.SJL-*Ptprc*^{a} *Pepc*^{b}/BoyJ (B6 CD45.1), and B6J.129(Cg)-Gt(ROSA)26Sor$^{tm1.1(CAG-cas9*,-EGFP)Fezh/J}$ (Cas9-GFP, BL/6J) were procured from The Jackson Laboratory. Primary murine leukemia cells (WT and Igf2bp3 KO) as previously described (6) were transplanted into busulfan-conditioned recipients. One week following transplantation, mice were injected with vehicle or I3IN-002, three times a week intraperitoneally, at a dose of 25 mg/kg, for three weeks, with an endpoint at four weeks post-transplantation. The peripheral blood engraftment of the leukemic cells was checked by FACS at week 2 and week 4. Once the peripheral blood engraftment reached >20% at 4 weeks, the experiment was terminated and tissues were harvested to be analyzed by FACS, histology and RT-qPCR. All of the animal experiments received Institutional Animal Research Committee approval at UCLA.

Cellular thermal shift assay (CETSA)

A cellular thermal shift assay was performed on SEM cells treated with the test compound, based on published protocols(11). Briefly, 20 $x10^6$ cells were treated with 25 µM concentration of test compound in 40 mL of complete growth media and incubated for 24 hour. at 37 ˚C in CO_2 incubator, DMSO was used as vehicle control. After incubation, cells were spun down and washed with PBS. Cells were further re-suspended in 1 mL of PBS with 1x protease inhibitor cocktail and 100 uL of cell suspension was distributed in individual PCR tubes. Cells were subjected to thermal denaturation at different temperature ranging from 38 ˚C – 52 ˚C on a thermal cycler for 3 minutes. Thermal treated cells were lysed by flash freeze and thaw cycle in liquid Nitrogen and cleared by centrifugation at 20,000xg for 20 minutes at 4 °C. Lysates were boiled in sample buffer and subjected to western blotting.

Drug Affinity responsive target stability (DARTS) assay

DARTS assay (12) was performed to study direct binding of I3IN-002 with IGF2BP3 protein. Briefly, $5x10^7$ SEM cells were lysed in 1 mL of m-PER buffer (Thermo scientific) and incubated on ice for 10 minutes. After incubation, lysate was centrifuged at 17,000xg for 10 min at 4^0C. The supernatant was transferred to a fresh tube and mixed with one-tenth of the 10x TNC buffer (500 mM Tris-HCl, pH 8.0, 500 mM NaCl and 100 mM $CaCl_2$), followed by protein estimation using the BCA assay. Approximately 50 µg of lysate was incubated with different concentrations of I3IN-002 (DMSO, 25, 50,100, 250 and 500 µM) for 1 hour, followed by pronase (Roche, 10,165,921,001) treatment (1:500) for 30 minutes at room temperature. The pronase activity was quenched by adding a protease inhibitor cocktail. The lysate was then boiled in 2x Laemmli buffer for 10 min at 90^0C and run on SDS PAGE. The membrane was the probed for IGF2BP3 and Actin beta for loading control.

Thermal Shift Assay (TSA)

Thermal shift assay (13) was performed using both full-length IGF2BP3 and RRM1-2 domain of IGF2BP3 purified protein. Briefly, 10 μM of purified protein was incubated with 100 μM of I3IN-002 for 30 minutes at room temperature. SYPRO dye (5000x) diluted in Bis-Tris buffer, pH 6.5 was added to the reaction mix. The reaction was run on a quantitative PCR machine (QuantStudio 3) using melt curve protocol.

Dual Luciferase Assay

Luciferase assay was performed using the Promega Dual-Luciferase Assay system on IGF2BP3 targets: CDK6, BCL2, HOXA9 and BNIP3L. The CDK6 3' UTR cloning was discussed previously (4). For BNIP3L, 486 bp of the BNIP3L 3'UTR beginning at chromosomal position chr8: 26,411,300; for the BCL2 3' UTR, approximately 591 bp beginning at chromosomal position chr18:63,128,033 were cloned into the pmirGlo vector. Next, 293T cells were co-transfected with the pmirGlo reporter construct and IGF2BP3 overexpression vector, with the reporter vector: overexpression vector ratio of 1:10 (50 ng:500 ng). Co-transfections were performed with BioT (Bioland) as per the manufacturer's instructions. Cells were lysed after 48 hours, Firefly and Renilla Luciferase substrate was added, and luminescence was measured on a Varioscan Lux (Thermo Scientific). The ratio of Firefly to Renilla luciferase activity was calculated for all samples and expressed as the Fold change from DMSO treatment for that particular reporter vector.

RNA isolation and qPCR

Previous protocols were adapted for RT-qPCR as standard procedures (7). A full list of RT-qPCR primers are presented in **Supp. Table 4**. For normalization to housekeeping genes, we used RT-qPCR primers for human 18S (or actin) and mouse L32.

RNA Sequencing.

Total RNA was extracted from cell pellets using Qiazol (Qiagen) per manufacturer's protocol with the following modification to include an additional RNA ethanol wash step: after the total RNA was solubilized in ddH_2O, one overnight ethanol precipitation step was included for further purification. Libraries for RNA-Seq were prepared with KAPA mRNA-Seq Hyper Prep Kit. The workflow consisted of mRNA enrichment and fragmentation, first strand cDNA synthesis using random priming followed by second strand synthesis converting cDNA:RNA hybrid to double-stranded cDNA (dscDNA), and incorporating dUTP into the second cDNA strand. cDNA generation was followed by end repair to generate blunt ends, A-tailing, adaptor ligation and PCR amplification. Different adaptors were used for multiplexing samples in one lane. Sequencing was performed on Illumina HiSeq3000 for a SE 1x50 run. Data quality check was done on Illumina SAV. Sample preparation and sequencing were completed by the UCLA Technology Center for Genomics & Bioinformatics (TCGB).

Bioinformatics Methods & Data Analysis

Following completion of sequencing and data quality check, demultiplexing was performed with Illumina Bcl2fastq v2.19.1.403 software. The reads were mapped by STAR 2.7.9a(14) and read counts per gene were quantified using the human genome GRCh38. In Partek Flow, read counts were normalized by CPM +1.0E-4. All results of differential gene expression analysis utilized the statistical analysis tool, DESeq2(15). P-value ($p<0.05$), FDR (<0.05), and fold change (FC>2-fold) filters were applied for differentially expressed gene lists prior to downstream analysis. Multiple testing correction was performed using the Benjamini–Hochberg method. Significant differentially expressed genes have adjusted *P* value =< 0.05 and absolute log2FC >= 1. Enrichment analyses were completed with Metascape (16).

RNA immunoprecipitation

RNA immunoprecipitation assay was performed on SEM cells treated with 5 μM concentration of I3IN-002 and DMSO for 48 hours. After incubation, cells were lysed in a non-denaturing lysis buffer supplemented with protease inhibitor and RNase inhibitor. Lysate was cleared at 12000 rpm for 15 minutes and RIP was performed on the cleared lysate by adding 5 μg of IGF2BP3 antibody/ IgG and 50 μL of Protein G agarose beads and incubated overnight at 4 degree Celsius.

Immunoprecipitation was confirmed by Western Blotting for IGF2BP3. RNA samples were isolated and subjected to either high throughput RNA-seq, or to directed RT-qPCR for known targets of IGF2BP3.

RIP-seq data analysis.

For RIP-seq, paired input and RIP samples were provided to the UCLA TCGB. Libraries for RNA-Seq were prepared with the ABclonal FAST mRNA Library Prep Kit. Following the same initial pipeline as for RNA-seq (see above), read counts were obtained as above. Next, DE-seq2 was used to compare RIP samples against input, for each of the two conditions, control (DMSO) versus I3IN-002 treatment, yielding high-probability enrichments (padj<0.01) and enrichment ratios (fold-changes). These enrichment ratios were compared between conditions to prepare scatter plots as shown. The ratio difference was calculated as enrichment ratio (I3IN-002)-enrichment ratio (DMSO). Genes that were enriched in DMSO-treated samples were compared against genes previously identified as targets of IGF2BP3 by eCLIP-seq analysis of SEM cells(17).

Statistical analysis

Data shown represents mean ± SD for continuous numerical data, unless otherwise indicated. Two-tailed student's *t* tests or one-way ANOVA followed by Bonferroni's multiple comparisons test were performed using GraphPad Prism software and conducted as described in the figure

legends. Survival analyses were performed using Kaplan-Meier method with comparisons made using log-rank tests, followed by Bonferroni's correction for multiple comparisons. A *P* value less than 0.05 was considered significant.

Additional reagents. Additional reagents and kits are listed in **Supp. Table 5**.

References:

1. Jaiswal AK, Truong H, Tran TM, Lin TL, Casero D, Alberti MO, et al. Focused CRISPR-Cas9 genetic screening reveals USO1 as a vulnerability in B-cell acute lymphoblastic leukemia. *Scientific Reports.* 2021;11(1):13158.
2. Sharma G, Tran TM, Bansal I, Beg MS, Bhardwaj R, Bassi J, et al. RNA binding protein IGF2BP1 synergizes with ETV6-RUNX1 to drive oncogenic signaling in B-cell Acute Lymphoblastic Leukemia. *J Exp Clin Cancer Res.* 2023;42(1):231.
3. Cheung LC, de Kraa R, Oommen J, Chua GA, Singh S, Hughes AM, et al. Preclinical Evaluation of Carfilzomib for Infant KMT2A-Rearranged Acute Lymphoblastic Leukemia. *Front Oncol.* 2021;11:631594.
4. Kasai F, Asou H, Ozawa M, Kobayashi K, Kuramitsu H, Satoh M, et al. Kasumi leukemia cell lines: characterization of tumor genomes with ethnic origin and scales of genomic alterations. *Hum Cell.* 2020;33(3):868-76.
5. Lechman ER, Gentner B, Ng SWK, Schoof EM, van Galen P, Kennedy JA, et al. miR-126 Regulates Distinct Self-Renewal Outcomes in Normal and Malignant Hematopoietic Stem Cells. *Cancer Cell.* 2016;29(4):602-6.
6. Lin TL, Jaiswal AK, Ritter AJ, Reppas J, Tran TM, Neeb ZT, et al. Targeting IGF2BP3 enhances antileukemic effects of menin-MLL inhibition in MLL-AF4 leukemia. *Blood Adv.* 2024;8(2):261-75.
7. Palanichamy JK, Tran TM, Howard JM, Contreras JR, Fernando TR, Sterne-Weiler T, et al. RNA-binding protein IGF2BP3 targeting of oncogenic transcripts promotes hematopoietic progenitor proliferation. *J Clin Invest.* 2016;126(4):1495-511.
8. Guha R. Exploring Structure-Activity Data Using the Landscape Paradigm. *Wiley Interdiscip Rev Comput Mol Sci.* 2012;2(6).
9. Tran TM, Philipp J, Bassi JS, Nibber N, Draper JM, Lin TL, et al. The RNA-binding protein IGF2BP3 is critical for MLL-AF4-mediated leukemogenesis. *Leukemia.* 2022;36(1):68-79.
10. Christen F, Hablesreiter R, Hoyer K, Hennch C, Maluck-Bottcher A, Segler A, et al. Modeling clonal hematopoiesis in umbilical cord blood cells by CRISPR/Cas9. *Leukemia.* 2022;36(4):1102-10.
11. Jafari R, Almqvist H, Axelsson H, Ignatushchenko M, Lundbäck T, Nordlund P, et al. The cellular thermal shift assay for evaluating drug target interactions in cells. *Nature Protocols.* 2014;9(9):2100-22.
12. Pai MY, Lomenick B, Hwang H, Schiestl R, McBride W, Loo JA, et al. Drug affinity responsive target stability (DARTS) for small-molecule target identification. *Methods Mol Biol.* 2015;1263:287-98.
13. Wu T, Hornsby M, Zhu L, Yu JC, Shokat KM, and Gestwicki JE. Protocol for performing and optimizing differential scanning fluorimetry experiments. *STAR Protoc.* 2023;4(4):102688.
14. Dobin A, Davis CA, Schlesinger F, Drenkow J, Zaleski C, Jha S, et al. STAR: ultrafast universal RNA-seq aligner. *Bioinformatics.* 2013;29(1):15-21.
15. Love MI, Huber W, and Anders S. Moderated estimation of fold change and dispersion for RNA-seq data with DESeq2. *Genome Biol.* 2014;15(12):550.

16. Zhou Y, Zhou B, Pache L, Chang M, Khodabakhshi AH, Tanaseichuk O, et al. Metascape provides a biologist-oriented resource for the analysis of systems-level datasets. *Nat Commun.* 2019;10(1):1523.
17. Sharma G, Gutierrez M, Jones AE, Kapoor S, Jaiswal AK, Neeb ZT, et al. IGF2BP3 redirects glycolytic flux to promote one-carbon metabolism and RNA methylation. *Cell Rep.* 2025:116330.

Supplemental Table 1. Reagents used in cell culture experiments.

Cell lines		
RS4;11	ATCC	CRL-1873
NALM6	ATCC	CRL-3273
SEM	DSMZ	ACC 546
REH	ATCC	CRL-8286
PER 785	Kids Cancer Centre, UWA, Perth Australia	
KASUMI-2	DSMZ	ACC 526
OCI-AML8227	Princess Margaret Cancer Centre, Toronto, Canada: Kind gift from Dr. John Dick.	
Media and supplements		
IMDM	Gibco	12440046
RPMI 1640	Gibco	11875119
FBS	Gibco	26140079
mSCF	Invitrogen	RP87738
IL-6	Gibco	PHC0065
hFLT-3	Gibco	PHC9415
mTPO	Invitrogen	RP87753
AMEM	Wisent	310-010 CL
BITS 9000	Stemcell Technologies	09500
R&D SCF	R&D Systems	11010SC010
R&D TPO	R&D Systems	288TP005
R&D FLT3-L	R&D Systems	308FK025
R&D IL-6	R&D Systems	206IL050
R&D IL-3	R&D Systems	203IL010
R&D G-CSF	R&D Systems	214CS005

Supplemental Table 2. Antibodies used in FACS, western blot and immunoprecipitation assays.

Antibodies		
Biolegend	105826	APC/Cyanine7 anti-mouse CD117 (c-kit)
Biolegend	118103	Biotin anti-mouse TCR γ/δ Antibody
Biolegend	312225	Brilliant Violet 711™ anti-human CD10 Antibody
Biolegend	157211	Pacific Blue™ anti-mouse CD45 Antibody
Biolegend	101318	PE/Cyanine7 anti-mouse CD16/32 Antibody
Biolegend	108124	PerCP/Cyanine5.5 anti-mouse Ly-6A/E (Sca-1)
Biolegend	343513	APC/Cyanine7 anti-human CD34 Antibody
Biolegend	303521	PerCP/Cyanine5.5 anti-human CD38 Antibody,
Biolegend	135120	Brilliant Violet 605™ anti-mouse CD117 (c-kit) Antibody
Biolegend	109815	Alexa Fluor® 488 anti-mouse CD45.2 Antibody
Biolegend	101215	PE/Cyanine7 anti-mouse/human CD11b Antibody
BD Bioscience	563973	Annexin V BV421
BD Bioscience	556463	Propidium Iodide solution
Proteintech	67447-1-Ig	cmyc monoclonal antibody
Fisher	50-173-2168	HOXA9 Rabbit anti-Human
Fisher	PIPA527978	CDK6 Polyclonal Antibody
Santa Cruz Biotech	sc-2357	mouse anti-rabbit IgG-HRP
Proteintech	146421AP150UL	rabbit anti-human igf2bp3
MBL	RN009P	MBL igf2bp3 rabbit anti-human/mouse
Sigma Aldrich	A5441	Actin beta Ab
Sigma Aldrich	F1804	Anti-FLAG Ab
Proteintech	674471IG150UL	Myc anti-human
Invitrogen	PA527978	CDK6 anti-human
Proteintech	185011AP150UL	HOXA9 rabbit anti-human
Invitrogen	PA527094	BCL-2 mouse anti-human
Proteintech	12658-1-AP	P4HA1 rabbit polyclonal anti-human
Proteintech	22339-1-AP	BTG2 rabbit polyclonal anti-human
Proteintech	12835-1-AP	KDM3A rabbit polyclonal anti-human

Supplemental Table 3. RNA Sequences used in IGF2BP3-RNA time resolved Forester resonance energy transfer assay.

RNA Oligo for FRET	Sequence
Unmethylated	5'biotin- CGU CUC GGA CUC GGA CUG CU-3'
Methylated	5'biotin- CGU CUC GG(m^6A) CUC GG(m^6A) CUG CU-3'

Supplemental Table 4. Quantitative PCR primers for genes assayed.

Gene name	Primer Sequence
Human	
TGFBR2-F	AAGATGACCGCTCTGACATCA
TGFBR2-R	CTTATAGACCTCAGCAAAGCGAC
BNIP3L-F	CAGCAATAATGGGAACGGGG
BNIP3L-R	ATCTTGTGGTGTCTGCGAGC
PAICS-F	CAC AGT GGT CTG AGG AAC AGC
PAICS-R	TAC AAT TCT GGG GCA ACC AGG
HMGA1-F	TTT TTC CTC TGT TCA CAA AC
HMGA1-R	AGC AGC AGC AAT GAC GGA TGT C
P4HA1 F	ATGACCCCTCGGAGACAGAA
P4HA1 R	GCCTCAGCCTTGGTTTTGC
MYC F	CCACAGCAAACCTCCTCACAG
MYC R	GCAGGATAGTCCTTCCGAGTG
CDK6 F	GCTGACCAGCAGTACGAATG
CDK6 R	GCACACATCAAACAACCTGACC
HOXA9 F	TGGACAGACTTAAATGCCCGC
HOXA9 R	TGAACCTATGATTGTAAGGAGCTG
BCL2 F	CGG TGG GGT CAT GTG TGT G
BCL2 R	CGG TTC AGG TAC TCA GTC ATC C
KDM3A F	CAGGAGCCACAGTAGGAGAC
KDM3A R	AGTTTGCCATCTCGCCTTGT
BTG2-F	ACCACTGGTTTCCCGAAAAG
BTG2-R	CTGGCTGAGTCCGATCTGG
RPS18 F	GAGGATGAGGTGGAACGTGT
RPS18 R	GGACCTGGCTGTATTTTCCA
Mouse	
Cdk6 F	TCTCACAGAGTAGTGCATCGT
Cdk6 R	CGAGGTAAGGGCCATCTGAAAA
Bcl2 F	GTC GCT ACC GTC GTG ACT TC
Bcl 2 R	CAG ACA TGC ACC TAC CCA GC
Hoxa9 F	AAAACACCAGACGCTGGAAC
Hoxa9 R	TCTTTTGCTCGGTCCTTGTT
Myc F	ATG CCC CTC AAC GTG AAC TTC
Myc R	CGC AAC ATA GGA TGG AGA GCA
Kdm3a F	TCGGAGACTTCTGGGATGGA
Kdm3a R	TTCAGTTTGCCATCTCGCCT
Bnip3l F	AGACCCGAAAACATCCCACC
Bnip3l R	CAGAAGGTGTGCTCAGTCGT
mRPS32-F	AAGCGAAACTGGCGGAAAC
mRPS32-R	TAACCGATGTTGGGCATCAG

Supplemental Table 5. Source of kits and reagents used as described in methods.

Kits and Reagents		
Promega	G8091	Caspase-Glo(R) 3/7 Assay, 10ml
Promega	G7572	CellTiter-Glo(R) Luminescent Cell Viability, 100m
Corning	21030CV	PBS
Thermo Scientific	EN0531	DNase free Rnase A
Invitrogen	NP0007	Invitrogen™ NuPAGE™ LDS Sample Buffer (4X)
Invitrogen	NP0002	Invitrogen™ NuPAGE™ MES SDS Running Buffer (20X)
VWR	101414-278	PerfeCTa® SYBR® Green FastMix®, ROX™
VWR	101414-106	qScript cDNA SuperMix, 5X, 100 rnxs
Thermo Scientific	78438	Protease inhibitor cocktail
Thermo Scientific	EO0381	RNase inhibitor
Sigma Aldrich	A2220	A2220 - ANTI-FLAG ® M2 Affinity Gel
Qiagen	12162	QIAGEN Plasmid Maxi Kit (10)
Qiagen	217004	miRNeasy Mini Kit (50)
Sigma Aldrich	B2635-10G	Busulfan
Sigma Aldrich	PPB019	Bis-Tris-Bicine-EDTA
Sigma Aldrich	11719408001	Protein A Agarose, 2 mL
StemCell Tech	3434	MethoCult
Promega	E2920	Dual-Glo® Luciferase Assay
Thermo Scientific	PV3965	LanthaScreen™ Tb-Streptavidin